



Multi-stage ultrahigh temperature metamorphism in the lower crust of the Kaapvaal craton recorded by U–Pb ages of garnet

Q. Shu^{1,2} · A. Beranoaguirre^{2,3} · R. Albert^{2,3} · L. J. Millonig^{2,3} · J. B. Walters² · H. R. Marschall^{2,3} · A. Gerdes^{2,3} · H. E. Hofer² · D. Hezel² · G. P. Brey²

Received: 4 March 2024 / Accepted: 13 March 2024
© The Author(s) 2024

Abstract

U–Pb ages were determined by split-stream LA-SF/MC-ICPMS in garnets from UHT granulite xenoliths (Star mine, South Africa; 124 Ma). They give a considerable age range of 400 million years with well-defined maximas at 3.09, 3.01 and 2.75 Ga. The oldest peak overlaps with the changeover from tonalites to K-granites at 3.14–3.04 Ga and with zircon ages of the mid-crustal granulites of the Vredefort dome (3.1 Ga) in the wake of the 3.2 Ga collision of three terrains that compose the Witwatersrand block. Subduction (or sagduction) of the uppermost crust in an ultrahot orogen setting brought shales and greenstones to the lower crust. Ultrahigh temperature (UHT) conditions are the result of high mantle potential temperatures and self-heating by the radioactive inventory of the subducted lithologies. Metamorphism, anatexis to very high degrees and melt extraction left UHT granulites as residue. Rejuvenation of UHT conditions was brought about by Dominion Group magmatism between 3.0 and 2.95 Ga. Magmatic uprise caused intense shearing in the lower crust followed by recrystallisation of the shear zones to generate the younger garnet age group. Ventersdorp flood basalt volcanism caused similar processes at around 2.72 Ga and generated the third garnet age group. Zircon gives U–Pb ages mainly around 2.72 Ga (both literature and our own data) i.e. zircon adjusted or newly crystallized at the youngest UHT event. Only few zircon grains retained older ages up to 2.94 Ga. Still unconstrained, but very high closure temperatures (≥ 1100 °C) for the U–Pb system in garnet keep the memory of the oldest ages in UHT granulites. Such ages can only be reset by recrystallization. This way, garnet records a prolonged high-temperature history of the lower crust of the Kaapvaal craton.

Keywords Kaapvaal craton · UHT granulite · U–Pb ages of garnet · Closure temperatures · LA-ICPMS

Introduction

The determination of the age and duration of metamorphism, especially of ultrahigh temperature (UHT) granulite-facies metamorphism, generally relies on accessory minerals such as zircon and monazite. Age interpretation with respect to

metamorphic stages and physical conditions is, however, not straightforward, because the latter are mainly derived from reactions of coexisting major minerals [see discussions by Harley et al. 2007; Kelsey and Hand 2015; Kohn et al. 2015; Harley 2016]. Zircon may grow along the prograde path and during peak metamorphism, but mostly forms at the onset of cooling along the retrograde path from trapped melt or from the release of Zr from other phases, such as garnet (Grt) and rutile (Rt) (Kelsey et al. 2008; Kohn et al. 2015; Yakymchuk 2023). In some cases, the growth sequence can be determined from micro-textures and microanalysis, coupled with considerations of mineral equilibria and trace-element distribution (Harley et al. 2007; Kohn 2016). Direct age determination of a rock-forming metamorphic mineral that can be used to derive pressure–temperature estimates was and is, therefore, highly desirable. Sm–Nd and Lu–Hf geochronology by isotope dilution mass spectrometry are commonly employed to date metamorphic garnet (see review in

Communicated by Dante Canil.

✉ G. P. Brey
brey@em.uni-frankfurt.de

- ¹ State Key Laboratory of Ore Deposit Geochemistry, Institute of Geochemistry, Chinese Academy of Sciences, Guiyang 550081, China
- ² Department of Geosciences, Goethe-University Frankfurt, Altenhöferallee 1, 60438 Frankfurt, Germany
- ³ Frankfurt Isotope and Element Research Center (FIERCE), Goethe-University Frankfurt, Frankfurt, Germany

Baxter and Scherer 2013). However, isotope dilution thermal ionization mass spectrometry (ID-TIMS) is a relatively slow, expensive, and laborious process that requires significant sample preparation to target specific growth domains (e.g. Pollington and Baxter 2010; Tual et al. 2022). Also, the ID-TIMS process involves the dissolution of large-volumes that may yield an average of different age domains or inclusions in minerals with no geological significance. Early on, U–Pb ID-TIMS geochronology studies were conducted on metamorphic garnets by Mezger et al. (1989, 1991). Later, DeWolf et al. (1996) pointed out that U-rich inclusions pose a problem in such studies. The challenges of ID-TIMS geochronology can be overcome by the high spatial resolution of laser ablation inductively coupled plasma mass spectrometry (LA-ICPMS) analysis combined with careful screening of time resolved signals and trace element contents. LA-ICPMS analysis is rapid, requires minimal sample preparation, and has a high spatial resolution. Examples are in-situ U–Pb age determinations on grossular-andradite garnets with 10–40 $\mu\text{g/g}$ (e.g. Seman et al. 2017), on amphibolite facies garnets with 0.2–694 ng/g by Schannor et al. (2021) and on pyrope–almandine garnets with < 90 ng/g U by Millonig et al. (2020). We push here the limits further to garnets with less than 15 ng/g .

Comparison of U–Pb age dating of garnet and zircon is especially critical for rutile-bearing UHT granulites. In zircon-quartz-bearing rocks at UHT metamorphic conditions, rutile has the capacity to host approximately 4000 $\mu\text{g/g}$ Zr at 900 °C and more than 10,000 $\mu\text{g/g}$ above 1000 °C (Watson et al. 2006). Garnet also can host several hundreds of $\mu\text{g/g}$ Zr at such extreme conditions (Kohn et al. 2015). Depending on bulk rock Zr-contents and the modal abundance of rutile, zircon can be present at peak metamorphic conditions or dissolved by incorporation into rutile and garnet. If bulk rock Zr-contents were high and modal abundances of rutile low, zircon will be stable at UHT metamorphic conditions. In the opposite case, zircon will grow on cooling by exsolution from rutile and garnet and reaction with quartz. It would thus postdate the time of peak metamorphism. Above the solidus, significant zircon dissolution into silicate melts is predicted for anatexis (Kohn et al. 2015; Yackymchuck 2023). High degrees of partial melting and near-complete melt extraction are required to generate nominally anhydrous UHT mineral assemblages. Therefore, zircon crystallization from remnant melt may be limited. The time difference between peak metamorphism and the new growth of zircon depends on the degree of Zr saturation in garnet and rutile amongst other phases, the cooling rate, and the respective closure temperatures. Short-lived UHT-metamorphism connected with fast cooling will diminish the time difference between peak metamorphic conditions and zircon ages. Mezger et al. (1989) estimated that garnet, zircon and monazite have a similar (high) closure temperature (T_c) in excess of 800 °C

for the U–Pb isotope system. Burton et al. (1995) estimated a similar closure temperature as Mezger et al. (1989), whereas Dahl (1997) estimated ≥ 1010 °C for garnet and ≥ 900 °C for zircon. Therefore, the U–Pb isotope record of garnet has a high potential to date the time of prograde and peak metamorphism, whereas zircon is more likely to record the subsequent stage of cooling in the metamorphic history of UHT granulites (Kohn and Kelly 2018). An example for the latter was described by Degeling (2002) from the Napier complex in Antarctica. Ubiquitous rutile cannot place any further constraints of the timing and duration of UHT metamorphism because of its low closure temperature for U–Pb (less than 600 °C; see e.g. Cherniak et al. 2007).

In our study, we test the ability of garnet U–Pb geochronology to date UHT metamorphism of lower crustal xenoliths from the Star mine kimberlite (age = 124 Ma) from the Kaapvaal craton. Schmitz and Bowring (2003a) measured U–Pb ages of various generations of zircon and monazite from UHT granulite xenoliths from Star and further three diamond mines on the Kaapvaal craton (details are described below). They obtained ages of ca 2.72 Ga for the main zircon population and considered this age to date the time of peak metamorphism of the granulites. This age correlates with the age of the Ventersdorp flood basalts, which erupted at 2714 ± 8 Ma throughout the central Kaapvaal craton (Armstrong et al. 1991). This large tectonomagmatic event was considered as causative for the UHT metamorphism with a duration of only 5–10 million years. Baldwin et al. (2007) obtained a maximum temperature of 1030 °C from Ti–zircon thermometry, which is lower than the estimated peak temperature from coexisting major minerals of > 1050 °C (appendix Fig. A1, simplified from Dawson et al. 1997). Therefore, zircon may not date the time of peak metamorphism, but rather the onset of cooling.

Repeated UHT metamorphism may have occurred, since widespread, high-temperature conditions existed in the crust already before 2.72 Ga. For example, granulite metamorphism occurred at 3.1 Ga at mid-crustal levels in the Vredefort Dome (Stevens et al. 1997; Hart et al. 1999; Moser et al. 2001) and in the Ancient Gneiss Complex in Swaziland (Suhr et al. 2015). Also, widespread granitic magmas, at least some of which were formed by crustal melting, intruded the Kaapvaal crust around that time (3.14–3.04 Ga) and dominate a large part of the Archean rock outcrop today (Eglington and Armstrong 2004; Marshall et al. 2010). Basaltic magmas erupted at the base of the Witwatersrand Basin at approximately 2.96 Ga (Paprika et al. 2021) and later in the middle of the Witwatersrand sequence around 2.90 Ga, coeval with the collision of the two main building blocks (Witwatersrand and Kimberley Block) of the Kaapvaal Craton (Fig. 1). Independent age information on the time of peak metamorphism is, therefore, highly desirable and the U–Pb isotope systematics of

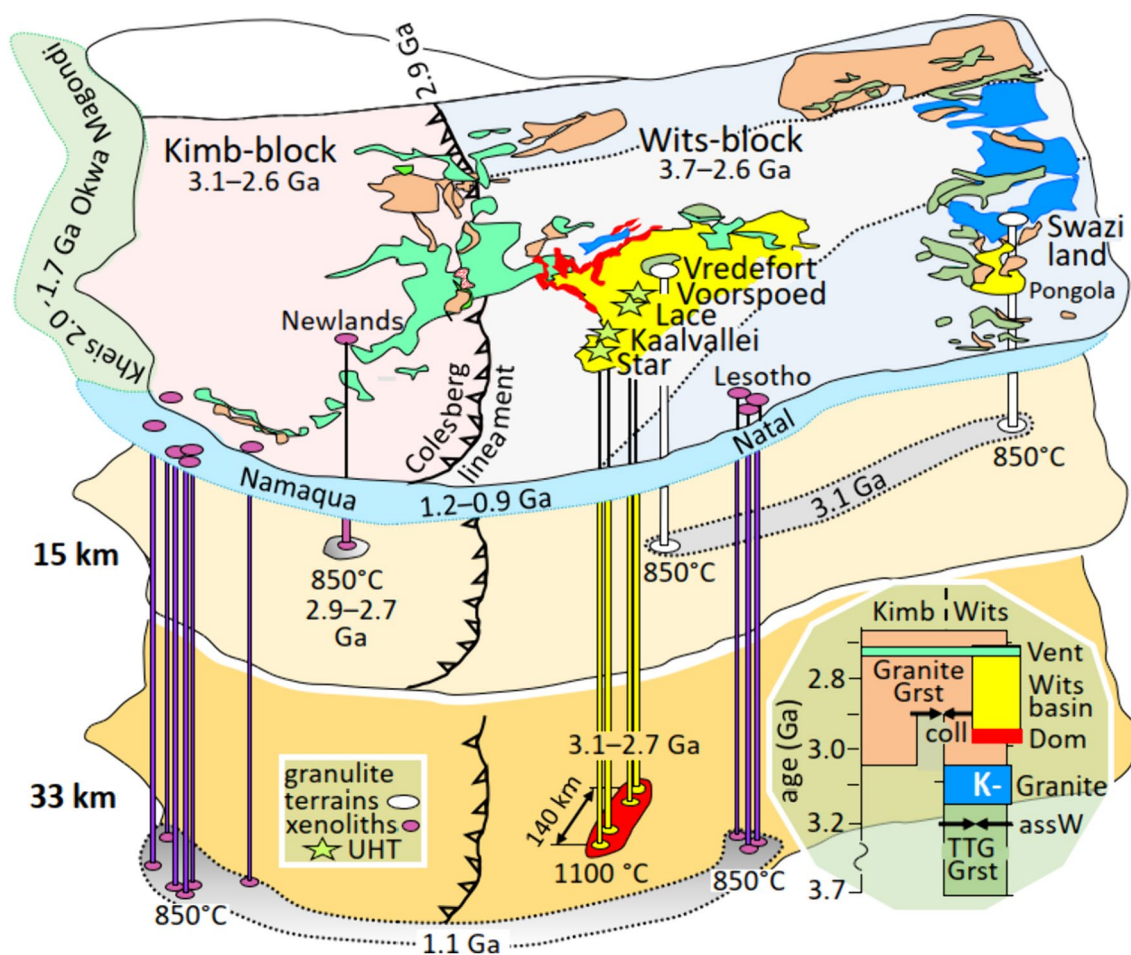


Fig. 1 Archean geology of the Kaapvaal craton (top plane) and location, age and conditions of origin of granulites. UHT granulites occur in kimberlites within the Witwaters-rand basin, granulites in kimberlites in and at the margin of the craton and in two uplifted terrains. The two planes at 15 and 33 km indicate the depth of meta-

morphism. Insert right: temporal evolution of the craton between 3.7 and 2.65 Ga. Wits= Witwatersrand block; Kimb= Kimberley block; Grst= Greenstone; Vent= Ventersdorp Group; Wits basin= Witwatersrand basin; Dom= Dominion Group; assW= assembly Witwatersrand block

garnet in metamorphic rocks offer such a possibility. We have collected UHT granulite xenoliths containing abundant pyrope–almandine garnet from the Star diamond mine in the Kaapvaal Craton with the aim of better constraining the time of peak metamorphism, reconstructing the early thermal evolution in the lower crust of an Archean craton and provide empirical constraints on Archean geodynamics.

An overview of the geology and granulites from the Kaapvaal craton

A simplified geological map of the Kaapvaal Craton and its granulite occurrences is shown in Fig. 1. The top plane is an oblique view of the Archean geology of the Kaapvaal Craton. It is summarized from the work of Eglington and Armstrong (2004) and Schoene et al. (2008). The main division of the Kaapvaal Craton is along the Colesberg lineament, where the older Witwatersrand Block in the east

and the younger Kimberley block in the west collided at approximately 2.9 Ga. The Witwatersrand Block consists of three 3.7–3.3 Ga old terrains (stippled lines in the figure) with tonalite-trondhjemite-granodiorite (TTG) gneisses and greenstone belts. The terrains amalgamated at approximately 3.2 Ga (Schoene et al. 2008). Subsequently, shield-wide crustal melting occurred at 3.14–3.04 Ga with the production of voluminous K-accentuated granitoids. The production of granitoid magmas continued until approximately 2.65 Ga. Basin formation began at approximately 2.99 Ga (Paprika et al. 2021) with the emplacement of the volcano-sedimentary Dominion Group at the base of the forthcoming Witwatersrand Basin. Its subsidence and that of the Pongola Basin lasted until 2.71 Ga. The Witwatersrand succession is interlaid by small-volume volcanics of the Crown and Bird lavas (Humbert et al. 2021). On the Kimberley Block, the oldest crustal rocks are 3.1 Ga old granitoids and greenstone belts. Granitoid formation continued until 2.7 Ga. Between

2.72 and 2.67 Ga, vast portions of the assembled Kaapvaal Craton were covered with the sediments and flood basalts of the Ventersdorp Supergroup. The periphery of the Kaapvaal Craton was reworked in the west between 2.1 and 1.8 Ga along the Kheis Magondi Belt (e.g., Altermann and Hälbig 1991) and in the south between 1.2 and 0.9 Ga along the Namaqua–Natal Belt (e.g., Thomas et al. 1993).

Granulites, metamorphosed at sub-UHT conditions, occur within and at the margin of the craton, whereas UHT granulite xenoliths are reported only from kimberlites within the Witwatersrand basin. Pelitic and mafic granulites outcrop in terrains within the Ancient Gneiss Complex in Swaziland (Suhr et al. 2015) and in an uplifted mid-crustal section of the Vredefort Dome (Stevens et al. 1997). Granulites are also sampled as xenoliths by the 114 Ma old Newlands kimberlite (Schmitz and Bowring 2003b). Peak metamorphic conditions were estimated at approximately 0.5 GPa and 850–950 °C for all occurrences by the authors cited above. Metamorphic zircon from the granulite terrains yielded U–Pb ages of approximately 3.1 Ga (Suhr et al. 2015), whereas rounded, oscillatory-zoned zircon inclusions in metamorphic minerals date to 3.5 Ga (Hart et al. 1999). Zircon and monazite from granulite xenoliths in the Newlands kimberlite are slightly discordant with upper and lower intercepts of 2.92 and 2.73 Ga, respectively (Schmitz and Bowring 2003b). The granulite xenoliths, entrained by kimberlites along the southern margin of the Kaapvaal craton, yield younger monazite and zircon ages between 1.1 and 1.0 Ga overlapping with the 1.2–0.9 Ga Namaqua–Natal belt (Schmitz et al. 2004; Sommer et al. 2013). Peak metamorphic conditions were between 800 and 900 °C at 1.0 to 1.3 GPa (Harte and Jackson 1981; Pearson et al. 1995; Schmitz and Bowring 2003b and references therein). The latter authors also provided discordant U–Pb ages on rutile, titanite and apatite from granulites and UHT granulites and constructed a thermochronological history of the craton. They suggest that resetting of rutile U–Pb systematics by thermal perturbations first occurred at around 2 Ga caused by the Bushveld intrusion and the impact of the Vredefort dome, followed by further resetting at around 1.2 (Namaqua Natal belt) and around 0.1 Ga caused by kimberlite volcanism.

UHT granulite xenoliths in the Kaapvaal Craton are reported from four kimberlite pipes that are aligned along the NNE trending axis of the Witwatersrand Basin (Fig. 1). They were first described by Dawson and Smith (1987) and Dawson et al. (1997) from the Lace diamond mine (133 Ma). Later, Schmitz and Bowring (2003a) reported similar UHT granulites from the other three Free State diamond mines Star (124 Ma), Kaalvallei (85 Ma) and Voorspoed (131 Ma) as well. Ages of kimberlites are taken from a review by Fields et al. (2008). The UHT granulites consist of garnet as the most abundant phase together with sillimanite (Sil), sapphirine (Spr), orthopyroxene (Opx), plagioclase (Pl) and

quartz (Qz) in various proportions and combinations (Fig. 2; Table 1). Dawson et al. (1997) compiled a petrogenetic grid from Hensen and Green (1973) and Bertrand et al. (1991) estimating that the paragenesis garnet + sapphirine + quartz is only stable at temperatures above 1050 °C and pressures between 1.0 and 1.3 GPa (Fig. A1 in the electronic appendix). Hensen and Green estimated somewhat lower pressures. Dawson et al. (1997) also used cordierite-bearing reaction coronas, the Fe–Mg partitioning between garnet and orthopyroxene, and Al-contents in orthopyroxene, to deduce that peak metamorphism was followed by near-isobaric cooling (appendix Fig. A1).

Three zircon types were distinguished by Schmitz and Bowring (2003a) and attributed to growth during prograde, peak and retrograde metamorphism (Type 1, 2, 3), respectively. Rare Type 1 zircon with oscillatory growth zones yielded the oldest U–Pb ages of 2.743 and 2.730 Ga, somewhat younger than a concordant U–Pb age of 2.767 Ga for monazite. Type 2 sector-zoned zircons have ages between 2.721 and 2.714 Ga. Pink-colored Type 3 zircon gave the youngest age of approximately 2.690 Ga. Type 3 zircon is related to leucosome textures and also occurs as overgrowths on colorless Type 2 zircon. Accordingly, the contemporaneity of the Type 2 zircons with the age of the Ventersdorp flood basalts at 2.714 ± 8 Ma (Armstrong et al. 1991) led the authors to suggest that the Ventersdorp magmatism caused UHT metamorphism and that UHT conditions lasted only for 5–10 Ma. Baldwin et al. (2007) calculated temperatures from the Ti-contents of Type 2 and Type 3 zircon (thermometer calibration of Ferry and Watson 2007) and obtained 880–1030 °C for Type 2 and 840–940 °C for Type 3 zircon, i.e. Type-2 zircon temperatures are lower than the peak metamorphic conditions inferred from the petrogenetic grid (Fig. A1).

Sample description

The Star mine is situated approximately 10 km northeast of Theunisson in the Free State of South Africa. Diamonds are mined from four east–west trending dikes of Group-II kimberlites with a K–Ar age of ca. 124 Ma (MacIntyre and Dawson 1976). Approximately 70 UHT granulite xenoliths with 3–4 cm in diameter were collected from a coarse concentrate dump during our field campaign. Most have broken surfaces, and a few have a kimberlite rim on one rounded side. Most samples have thin alteration rims along grain boundaries and some have larger, patchy alteration parts. We prepared 70–80 µm thick polished sections from 27 samples and selected 22 for electron probe microanalysis (EPMA). Mineral associations in each sample and estimated modal abundances are given in Table 1.

Garnet grains are elongated with embayed or irregular surfaces in a number of samples, but most are roundish and

Table 1 Modal and compositional characteristics of UHT granulites

Nr	Grt (vol%)	Grt MgO (n)	Spr MgO (n)	Pl CaO (n)	Qtz	Sil	Crn	Sp	Rt	S*	Gr
ST4	50	14.2±0.2 (12) poik. core	15.7 (2)	8.7±0.2 (3)	X	X		X	X	X	
ST7	45	14.8±0.1 (9)	15.5±0.3 (4)		X	X		X	X	X	X
ST8	30	14.5±0.3 (8)	15.7±0.1 (5)	9.4±0.2 (4)	X	X			X	X	
ST65	80	14.4±0.3 (5) poik. core	16.0 (1)	8.6±0.5 (2)	X	X		X	X	X	
ST68	60	14.6±0.2 (12) 13.2±0.9 (4)	15.6±0.3 (4)	8.6±0.2 (8)	X	X	X	X	X	X	X
ST69	50	14.6±0.5 (6) poik. core	15.5±0.4 (5)	8.1±0.3 (2)	X	X	X	X	X	X	
ST63		14.6±0.14 (9)	15.7±0.6 (5)	7.7±0.4 (15)	X	X	X		X	X	
ST1	70	13.7±0.2 (14)		8.5±0.1 (6)	X	X		X	X	X	
ST2	40	11.1±0.5 (4)		6.5±0.4 (3)	X	X			X	X	
ST3	35	13.0±0.2 (7)				X			X	X	
ST6	50	14.1±0.2 (17)		8.5±0.2 (10)	X	X		X	X	X	X
ST10	50	18.6±0.2 (11)		9.1±0.3 (6)	X	X			X	X	X
ST14	50	14.3±0.1 (9) poik. core			X	X			X	X	
ST58	80	14.3±0.2 (9) poik. core		8.5±0.3 (6)	X	X			X	X	
ST62	80	12.8±0.2 (8)		9.8±0.2 (3)		X	X	X	X	X	
ST64	60	12.8±0.1 (13) poik. core		8.1±0.2 (4)					X	X	X
ST12		10.3±0.3 (6)		10.4±0.5 (16)	X	X			X	X	
ST61		7.2±0.1 (7)		8.1±0.9 (12)	X	X	X		X	X	
ST70		11.8±0.3 (8)		7.6±0.4 (11)	X	X			X	X	
ST66		14.6±0.3 (13)		8.6±0.4 (10)	X	X	X		X	X	
ST5		7.3±0.1 (9)									
ST9		13.2±0.2 (16)		9.1±0.4 (11)	X	X			X	X	

* The modal amount of garnet (vol%) was estimated for most samples in thick sections by point counting with a 0.7 mm grid (column 2). The presence of poikiloblastic inclusions in garnet cores is indicated by “poik. core”, and the presence of all other phases is provided in columns ‘quartz’ to ‘graphite’ by the symbol X. Columns 3–5 give the mean MgO contents (in wt%) of garnet and sapphirine and the CaO contents of plagioclase together with the 2σ deviation and the number of analyses (n)

S sulfide

equigranular with 1–4 mm in diameter (Fig. 2a, b). Photomicrographs of all samples are shown in the Appendix in Fig. A2. Garnet abundances range from 45 to 80 vol%, estimated by point counting with a 0.7 mm grid (Table 1). Garnets from six samples have circular cores of mostly altered, ovoid inclusions (Fig. 2a). In some cases, quartz, rutile, plagioclase and rounded sulfide grains can be identified. Tiny, evenly distributed rutile needles (5–50 μm long and 1–2 μm thick; Appendix Fig. A2) are visible under the microscope in garnet grains from several samples. Examples for retrograde growth of garnet and of corundum are shown in Fig. 2c, d. Dawson and Smith (1997) describe a number of further reactions with retrograde growth of garnet.

Sapphirine occurs in nine samples. It is greenish with irregular shapes and with visually estimated abundances of up to 10 vol%. An example is shown in Fig. 2b, where

sapphirine is in direct contact with garnet, sillimanite and quartz. Other examples can be found in the Appendix in Fig. A2.

Plagioclase is present in most xenoliths with visually estimated 1–2 vol%. Sample ST2 has the highest abundance with ca. 10 vol%. Plagioclase was not found in four samples. It was either not present in the original rock or was completely altered by the kimberlite host magma.

Sillimanite and quartz are common in all samples with varying abundances from high to low, whereby quartz seems to be absent in four samples.

Primary spinel was found in eight samples. Ruby (Crn) occurs in retrograde reaction patches (Fig. 2d) of six samples. Large graphite (Gr) flakes (Fig. 3a) are clearly visible in five samples under a stereo microscope and in reflected light. Twelve further samples have rare, smaller graphite

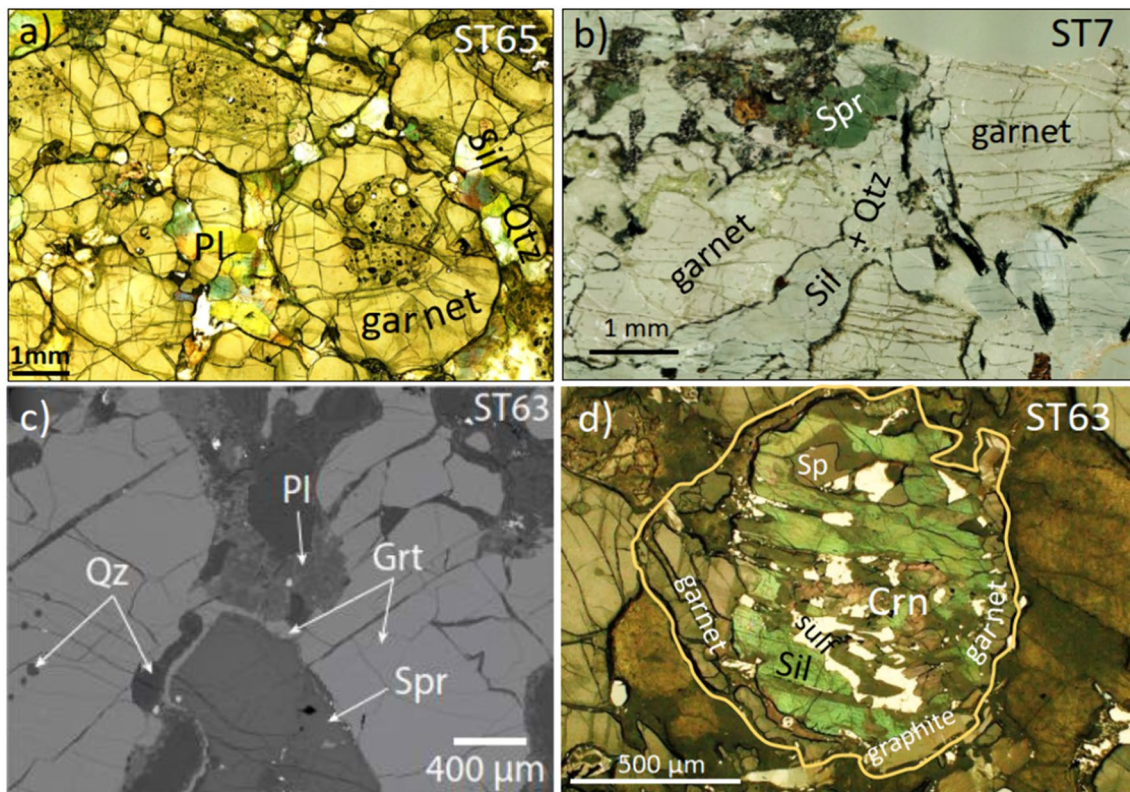


Fig. 2 **a** Sapphirine-bearing sample ST65 with roundish garnet grains and pokiloblastic inclusions in the cores. Plagioclase (Pl), quartz and sillimanite occur interstitially. **b** Sapphirine-bearing sample ST7 with elongated and irregularly embayed garnet grains. Flaky green sap-

phirine in contact with garnet, quartz, and sillimanite. **c** Growth of garnet between sapphirine and quartz. **d** Retrograde growth of corundum in sillimanite. The latter is mantled by retrograde garnet

flakes and graphite was not found in the other five samples. Rutile (Rt) and sulfide occur in all samples. Rutile grains reach more than 1 mm in size and can comprise up to approximately 3 vol% of the rock mode (visual estimate). It occurs as interstitial grains and as inclusions in garnet and sillimanite. Sulfide grains with amoeboid shapes occur interstitially and as roundish inclusions in garnet and sillimanite (Fig. 3a–d). The sulfide grains are mostly fresh, and only a few are slightly oxidized along their rims. Only one large zircon grain was found optically in sample ST7 (Fig. 3a, e). Otherwise, zircon was found by BSE and CL imaging in the matrix (Fig. 3e–g) and as inclusion in garnet and sillimanite (Fig. 3j–l). Graphite, sulfides and rutile can occur in direct contact with one another (Fig. 3a).

Analytical methods

Electron probe microanalysis (EPMA)

Major and minor element contents of silicates and oxides as well as the oxidation state of garnet were determined by EPMA in the wave-length-dispersive mode (WDS) with a

JEOL JXA-8530F Plus Hyperprobe equipped with a field emission gun at Goethe-University Frankfurt. Measuring procedures and conditions are described for silicates and oxides in the electronic appendix in file “EPMA analytical methods” and for Fe^{3+} determination in Höfer and Brey (2007) and Höfer et al. (2017).

Trace element and isotope determination by LA-ICPMS

Simultaneous U–Pb isotope and trace element analysis of garnet and sillimanite via split stream LA-(ICPMS + MC-ICPMS)

U–Pb isotopic and trace element data were acquired on garnet and, in some cases, on sillimanite from polished thick sections at Goethe-University Frankfurt (Frankfurt Isotope and Element Research Center, FIERCE). For the split-stream technique, we coupled a RESOLUTION-LR (Resonetics) 193 nm ArF Excimer laser (CompexPro 102, Coherent) equipped with an S-155 two-volume ablation cell (Laurin Technic, Australia) to two ICPMS instruments. The U–Pb data was collected with a multi-collector (MC)-ICPMS

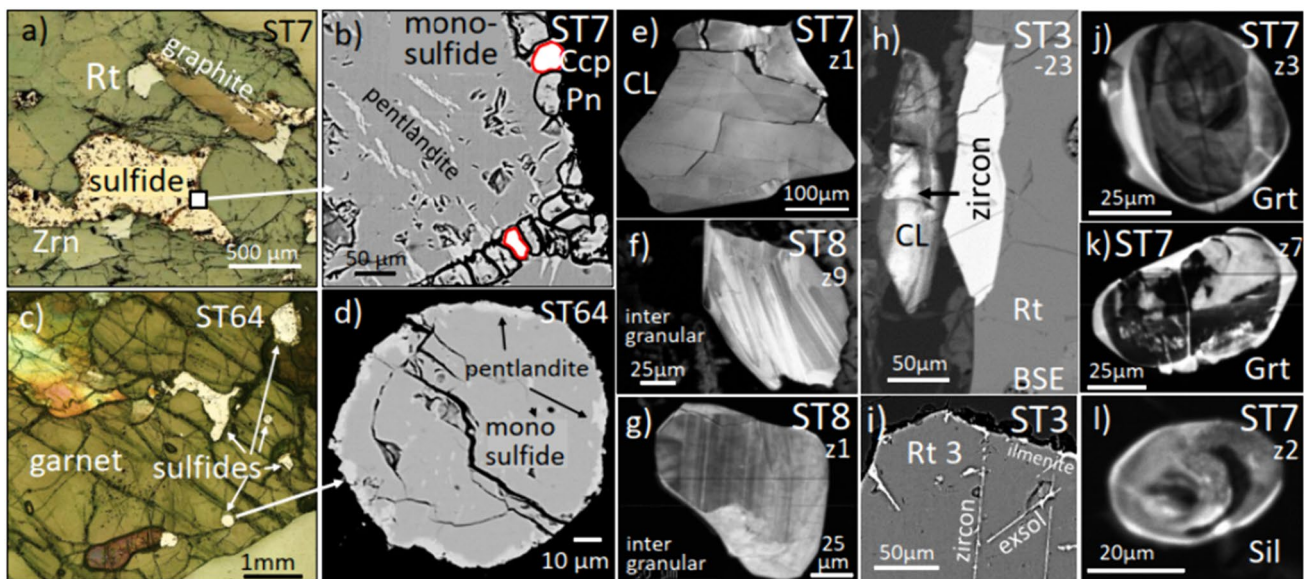


Fig. 3 **a** Large graphite flake intergrown with rutile and monosulfide. The large amoeboid monosulfide below is in contact with a large zircon (Zrn z1) and rutile. **b** BSE image of a section of that monosulfide. Small globular grains of mainly pentlandite and little chalcopryrite (Ccp) are aligned along cracks and rim. Feathery pentlandite exsolutions occur within the monosulfide. **c** Intergranular amoeboid monosulfides and globular monosulfide inclusions in garnet. **d** Glob-

ular monosulfide with pentlandite exsolutions mainly along the rim. **e–g** Cathodoluminescence (CL) images of intergranular zircons. Zircon ST7z1 shows no zonation, ST8z1,9 are complexly zoned. **h** BSE and CL picture of zircon ST3-23 intergrown with rutile. **i** Rutile with ilmenite rim and zircon exsolutions. **j–l** CL pictures of roundish zircon grains with complex zonation included in garnet or sillimanite

(Neptune Plus, ThermoFisher Scientific), while the trace element data was simultaneously analyzed with a single-collector (SC)-ICPMS (Element XR, ThermoFisher).

Due to the low U contents of garnet of only a few ng/g, 80% of the ablated material was used for U–Pb analysis while the remaining 20% were used for trace element analysis. This ratio was achieved by using different tubing diameters and lengths. After the ablation cell, the particle stream was divided via a small glass chamber with two outlets, four-fifths of the material was directed to the MC-ICPMS (U–Pb) and the rest to the SC-ICPMS. Analytical details (i.e. gas flows, spot sizes, etc.) are detailed in Appendix Table A1. The U–Pb analyses followed the procedure described in Beranoaguirre et al. (2022). Soda-lime glass SRM NIST614 (Jochum et al. 2011) was used as the primary reference material to correct for mass bias, inter-element fractionation and instrumental drift during the analytical session. Mali garnet reference material (Seman et al. 2017) was used to correct the matrix offset between NIST glass and garnet. Lake Jaco (Seman et al. 2017) and an in-house grossular-andradite garnet (reproducible age ca. 45 Ma) were measured repeatedly during each analytical session to validate the analysis. All details of the measuring procedure and the results for the reference materials in each session are reported in Appendix Table A1 (MetaData).

Data processing was done with an in-house VBA Microsoft Excel® spreadsheet (Gerdes and Zeh 2006, 2009),

which employs the same algorithms as Isoplot (Ludwig 2012). Uncertainties are the quadratic additions of internal uncertainties, counting statistics, background, and the excess of variance (Horstwood et al. 2016). Data are displayed in Tera-Wasserburg plots (Tera and Wasserburg 1972) and ages were calculated by unanchored regression as lower Concordia-curve intercepts. Expanded systematic uncertainties are also reported. During data processing, the U, Pb and trace element data of each analysis was scrutinized for inclusions of zircon, monazite, rutile, sillimanite and contamination by kimberlite, reflected by elevated Zr, REE (especially Ce), Ti, Sr and LREE (see below “Garnet U–Pb ages”).

For trace element analysis, ^{29}Si in garnets was used as an internal standard and SRM NIST614 glass (Jochum et al. 2011) and BIR-1 basaltic glass (Jochum et al. 2016) as external reference materials. The trace element data was evaluated using LADR (Norris Scientific, Norris and Danyushkevsky 2018).

LA-ICPMS analysis (zircon)

Uranium-Pb and trace element data of zircon were measured from polished thick sections in a separate analytical session using the (SC)-ICPMS coupled to the Excimer laser described above. All analytical details are specified in the Appendix in Table A2. The reference zircon GJ-1 (Jackson et al. 2004; 603 Ma; ID-TIMS data, Wolfgang Dörr, pers.

comm.) was analyzed repeatedly to correct for the laser- and plasma-induced elemental fractionation and the instrumental mass bias (i.e. $^{207}\text{Pb}/^{206}\text{Pb}$ and $^{206}\text{Pb}/^{238}\text{U}$ ratios). Secondary reference zircon BB-16 (Santos et al. 2017), and Plesovič (Slama et al. 2008) were used for quality control. Raw data were corrected with the same VBA Microsoft Excel® spreadsheet as the garnet U–Pb data. The trace element data were processed using LADR following the method described in Kozlik et al. (2016).

Results and interpretation

Major and minor element composition of phases

Garnet grains were analyzed in intervals from core to rim with 4–17 points per probe mount. Averages for MgO together with the number of analyses (n) are given in Table 1. Selected analyses corresponding to averages are given in the appendix (Table A3). In general, there are no systematic compositional variations from core to rim and garnet from within inclusion coronas is not different to that from outside. The MgO contents range from 7.2–18.6 wt% with 82% falling between 12.8 and 14.7 wt% (Table 1). The 2σ deviation on the average for each sample is 0.1 wt% for 50% of the samples, 0.2 wt% for 27% and 0.3 wt% for 23%. The range of CaO contents is very limited between 1.2 and 1.8 wt%, generally with a variability of ± 0.1 wt% and in a few cases of 0.3 to 0.6 wt%. In such cases, CaO is slightly negative correlated with MgO, the latter with a much smaller variability.

The Fe-oxidation state in garnet was determined in four samples (Table 2). They give consistently a $\text{Fe}^{3+}/\Sigma\text{Fe}$ ratio of zero meaning that no andradite component is present in the garnets. MnO is always around 0.3 wt% so that garnet is mainly an almandine–pyrope solid solution in roughly equal proportions with only approximately 3 mol% grossular. Mg-values ($100 \times \text{Mg}/(\text{Mg} + \text{Fe})$) range from 45 to 53 in sapphirine-free samples and approximately 54–55 in sapphirine-bearing samples (Fig. 4a). TiO_2 contents range from 0.05 to 0.30 wt% and vary within ± 0.05 wt% in individual samples, i.e. within the analytical error. Only a few analyses show a larger deviation that may be caused by the inclusion of small rutile needles in the analysis.

Table 2 Fe-oxidation state of garnet

Sample	ST3	ST6	ST65	ST68
FeO (wt%)	22.57	21.76	21.01	20.99
$\text{Fe}^{3+}/\Sigma\text{Fe}$	0.003	–0.003	0.005	0.005
Detection limit $\text{Fe}^{3+}/\Sigma\text{Fe}$ in garnet = 0.010				

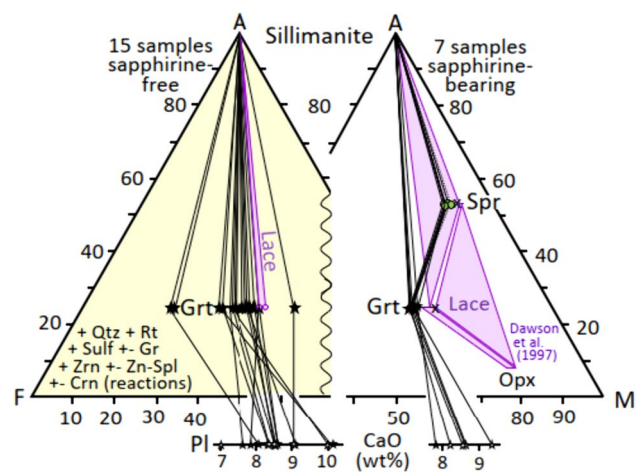


Fig. 4 AFM (Al_2O_3 –FeO–MgO) diagrams for 15 sapphirine-free and 7 sapphirine-bearing samples. The compositions of garnet, sillimanite and sapphirine from Star are shown in black and (for comparison) those from Lace in violet (Dawson et al. 1997). The latter also include Opx-bearing varieties. The bars outside the triangles show the CaO-contents of plagioclase from Star. Tie lines connect the CaO contents of plagioclase with the composition of coexisting garnet in the AFM diagrams

Sapphirine was analyzed with 1 to 5 spots in each sample (variability for MgO in Table 1). Averaged analysis are given in the appendix (Table A3). Mg-values range from 76 to 78 as shown in Fig. 4a. Like in the Lace UHT granulites reported by Dawson and Smith (1987) and Dawson et al. (1997), Cr_2O_3 in sapphirine in this study is high and exceeds 1.2 wt% in all cases. The comparison of the mineral compositions shows that Lace garnet and sapphirine have slightly higher Mg-value for both the sapphirine-free and the sapphirine-bearing varieties compared to Star (Fig. 4a). We did not find any orthopyroxene (Opx) in our samples, whereas Opx-bearing samples were previously reported from the Lace diamond mine (Fig. 4; Dawson and Smith 1987).

Plagioclase was analyzed with 2–10 spots per sample. The variability of CaO contents is given in Table 1. The internal 2σ variability of each sample is 0.2 wt% in most cases, 0.3–0.5 wt% in a few cases and 0.9 wt% in one extreme case. Averaged CaO contents vary between 7.7 and 10.4 wt% corresponding to An_{31-38} . They are shown in Fig. 4 on separate bars outside the AFM diagrams. With one exception, garnet with lower Mg# coexists with plagioclase with lower CaO content. Averaged plagioclase analyses are given in Appendix (Table A3).

Sillimanite is present in all samples but was analyzed only in nine. The mean minor element content is 0.15 wt% TiO_2 , 0.24 wt% FeO and 0.47 wt% Cr_2O_3 . Spinel (Spl) grains are present in seven samples and are Cr, Zn and V rich like those from the Lace UHT granulites (Dawson et al. 1997). Ruby in reaction haloes from three samples contains approximately 0.04 wt% TiO_2 , 0.93 wt% Cr_2O_3 and 0.27 wt% FeO.

Zircon inclusions in garnet and sillimanite and zircon grains in the matrix were analyzed in three samples by EPMA (two sessions separated by several weeks). During the first session (EPMA1) 28 grains were analyzed with 2–8 points in each grain depending on its size. Analyses of zircons intergrown with or adjacent to rutile were rejected because of artificial high Ti due to phase boundary fluorescence. For the accepted 122 analyses Ti varies between 142 and 186 $\mu\text{g/g}$ (Fig. 5a). Selected analyses are given in the appendix (Table A5). U–Pb isotope analysis was carried out on the same grains (see below) followed by fourteen LA-ICPMS analysis of trace elements (see below). The fragments of these zircons were analyzed by EPM in a second session (EPMA2). The Ti-content for 18 analyses ranged from about 65–145 $\mu\text{g/g}$; Table A5).

Rutile is in some cases intergrown with zircon (Fig. 3h), commonly has zircon exsolutions and occasionally ilmenite seams along the rim (Fig. 3i). Zr contents in large rutile grains are shown in Fig. 5b as line profiles and as individual data points for rutile inclusions and exsolutions in garnet. Zirconium varies between 200 and 600 $\mu\text{g/g}$ in the large rutile grains (line profiles) and reaches up to 3700 $\mu\text{g/g}$ in rutile inclusions in garnet. Selected analyses are given in the appendix (Table A6).

Sulfides are almost Co-free monosulfides with small globular grains of pentlandite (Pn) and rare chalcopyrite (Ccp) aligned along cracks and rims and feathery pentlandite exsolutions within grains (Fig. 3b, d). Two pyrite grains were found in sample ST10 which coexist with an exsolved monosulfide with $\text{mss:Pn} = 50:50$, i.e. the primary monosulfide was significantly Ni-richer than all other monosulfides in the samples. Selected compositions are given in the appendix (Table A7). Forty two monosulfide analyses vary within the range of close to zero up to 15 at% Ni/(Fe + Ni), the field shown in Fig. 6a. The amount of pentlandite exsolutions

is estimated to be a maximum of 5 vol%, such that the preserved composition of the monosulfides is close to their original composition. The analysis of uncontaminated pentlandite was difficult because of the small size of the feathery exsolutions. Eighteen analyses give a range between 30–56 at% Ni/(Fe + Ni), close to the field of first appearance of pentlandite at ca. 550 °C according to Firdu and Taskinen (2010; Fig. 6a). A similar temperature is suggested by the comparison of chalcopyrite compositions with the phase diagram by Yund and Kullerud (1966; Fig. 6b).

Rare earth elements in garnet and zircon

Trace elements, along with a number of major elements, were analyzed in garnet simultaneously with the U–Pb isotopes. Accordingly, this yielded 50–60 analyses for each sample randomly distributed over multiple garnet grains. The full set of trace elements is given in the appendix (Table AX trace elements garnet). Examples of laser pits are shown in Fig. A2 for samples ST2, ST3 and ST6. By checking for anomalies of one or more elements in the time-resolved analytical spectra during offline data evaluation we were able to identify outliers for the U–Pb isotope systematics caused by impurities and inclusions (see below in ‘Garnet U–Pb ages’). Like the major elements, the trace elements are only slightly heterogeneous with no discernable systematic spatial variations, e.g. the range of heterogeneity for HREE contents within each sample lies at a factor of 1.5–2.0. Figure 7a shows the averaged chondrite-normalized REE pattern of six samples as representatives for all samples (data in Appendix Table A4). The LREE are strongly depleted with La down to 0.1 times chondritic, whereas the middle to heavy REE patterns are flat to slightly negatively inclined with abundances of 20–60 times that of CI chondrites. Garnet has pronounced

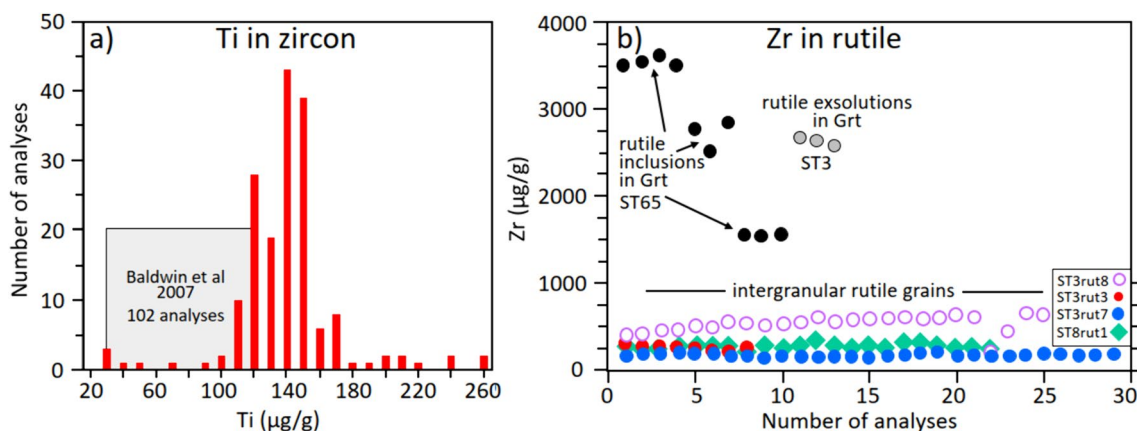


Fig. 5 **a** Histogram of the Ti-contents in zircon from samples ST3, ST7 and ST8 in comparison with the results of Baldwin et al. from Lace and Voorspoed (grey box). **b** Line profiles of Zr through four

intergranular rutile grains of two samples plus Zr contents of rutiles included in garnet (ST65) and of rutile exsolutions in ST3 garnet

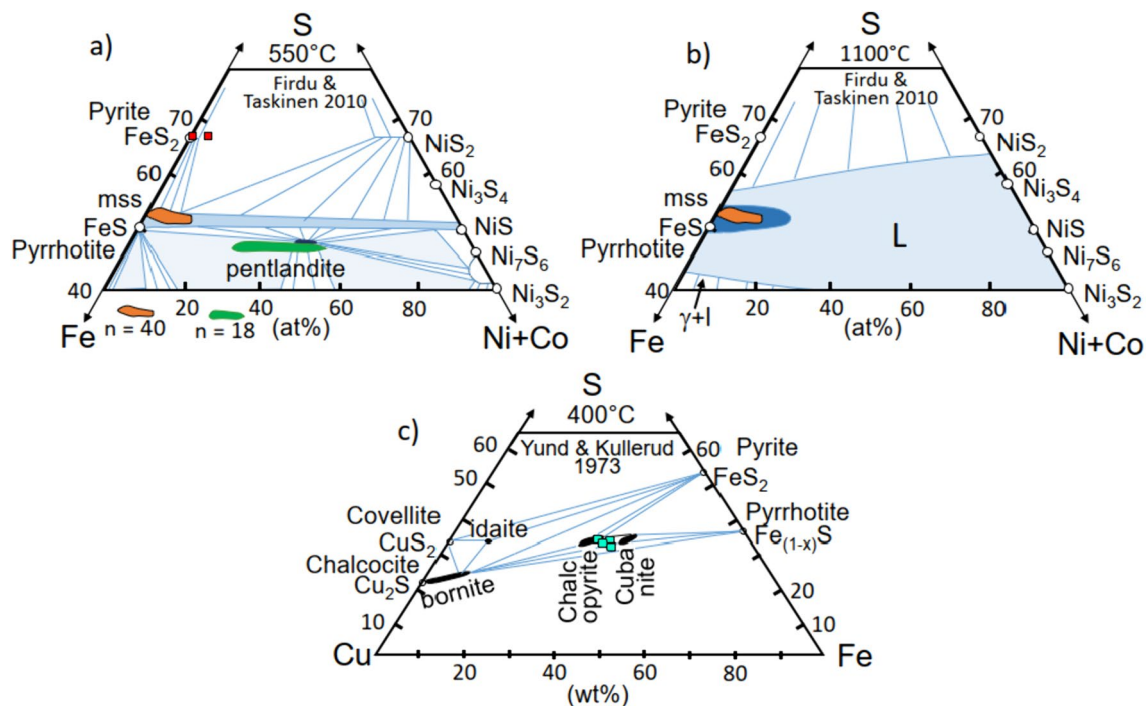


Fig. 6 Sections of the phase diagrams of the Fe(Ni, Co)S system at 1 atm at 550 and 1100 °C with tie lines and ternary fields from a compilation by Firdu and Taskinen (2010), based on Kullerud et al. (1969). **a** Averaged compositions of two line profiles of two pyrite grains in ST1 together with the fields of 42 monosulfide and 18 pentlandite analyses on several grains each from samples ST1, ST7, ST64, ST10 with tie lines and ternary fields for 550 °C. Pentlandite appears at about this temperature on cooling. **b** The phase diagram at 1100 °C after Firdu and Taskinen (2010). The field of monosulfides overlaps

with the field of residual monosulfides (blue field) within the large field of melt (light blue) in the intermediate portion of the Fe–Ni–S system at 1100 °C. Because of the small amounts of pentlandite (and chalcopyrite) exsolutions (Fig. 3b, d), the composition of monosulfide is close to the pre-exsolution composition. **c** The composition of four chalcopyrite grains from sample ST7 (Fig. 3b) in comparison with the phase diagram for Cu–Fe–sulfides as given by Yund and Kullerud (1966) for 400 °C

negative Eu anomalies ($\text{Eu}/\text{Eu}^* = 0.02\text{--}0.21$), consistent with the presence of plagioclase. The one garnet REE pattern given by Dawson et al. (1997) from Lace lies at the upper end of the range of garnet patterns of this study. The middle to heavy REE patterns of bulk rocks from Lace, Voorspoed and Star reported by Schmitz and Bowring (2003a) are similarly sloped to those of the garnet investigated here, but at overall lower abundances (Fig. 7a). The LREE contents in the bulk samples are elevated most likely as the result of contamination by the kimberlite host magma.

The REE patterns of zircon fall into two groups (Fig. 7 and Table A8). Eight analyses of three matrix and one inclusion (ST3-z23) grain have flat middle to heavy REE patterns with negative Eu- and positive Ce-anomalies (Fig. 7b). This figure also shows the range of garnet compositions from Fig. 7a for comparison. Four zircon inclusions in garnet and sillimanite have positively sloping REE patterns with negative Eu- and positive Ce-anomalies similar to matrix grains. All zircon grains analyzed for REE fall in a narrow age range between 2.68 and 2.73 Ga

except for grain ST7-z4 that yielded the oldest age of 2.94 Ga (see below “Zr U–Pb ages”).

Garnet U–Pb ages

We analyzed 16 samples in four different sessions (Table A1). Two were analyzed by LA-SF ICPMS and fourteen samples by LA-SF/MC ICPMS in three further analytical sessions separated by several weeks (electronic Appendix Table A1). Samples ST6 and ST14 were analyzed twice in different sessions to test the reproducibility of our analytical procedure. The ages derived from the two sessions (seq 2, 4) overlap within their uncertainties (2σ). We calculated weighted averages and use these ages further on (Table 3). Two samples (ST 2 and 8) were analyzed by laser ablation SF-ICPMS only, without simultaneous trace element analysis (cf. Millonig et al. 2020).

Approximately 60 analyses were collected for each sample. The U–Pb data points form linear arrays in $^{207}\text{Pb}/^{206}\text{Pb}$ vs. $^{238}\text{U}/^{206}\text{Pb}$ space mostly with nil to ten outliers per sample. All data are given in the Appendix in Table A1 and are

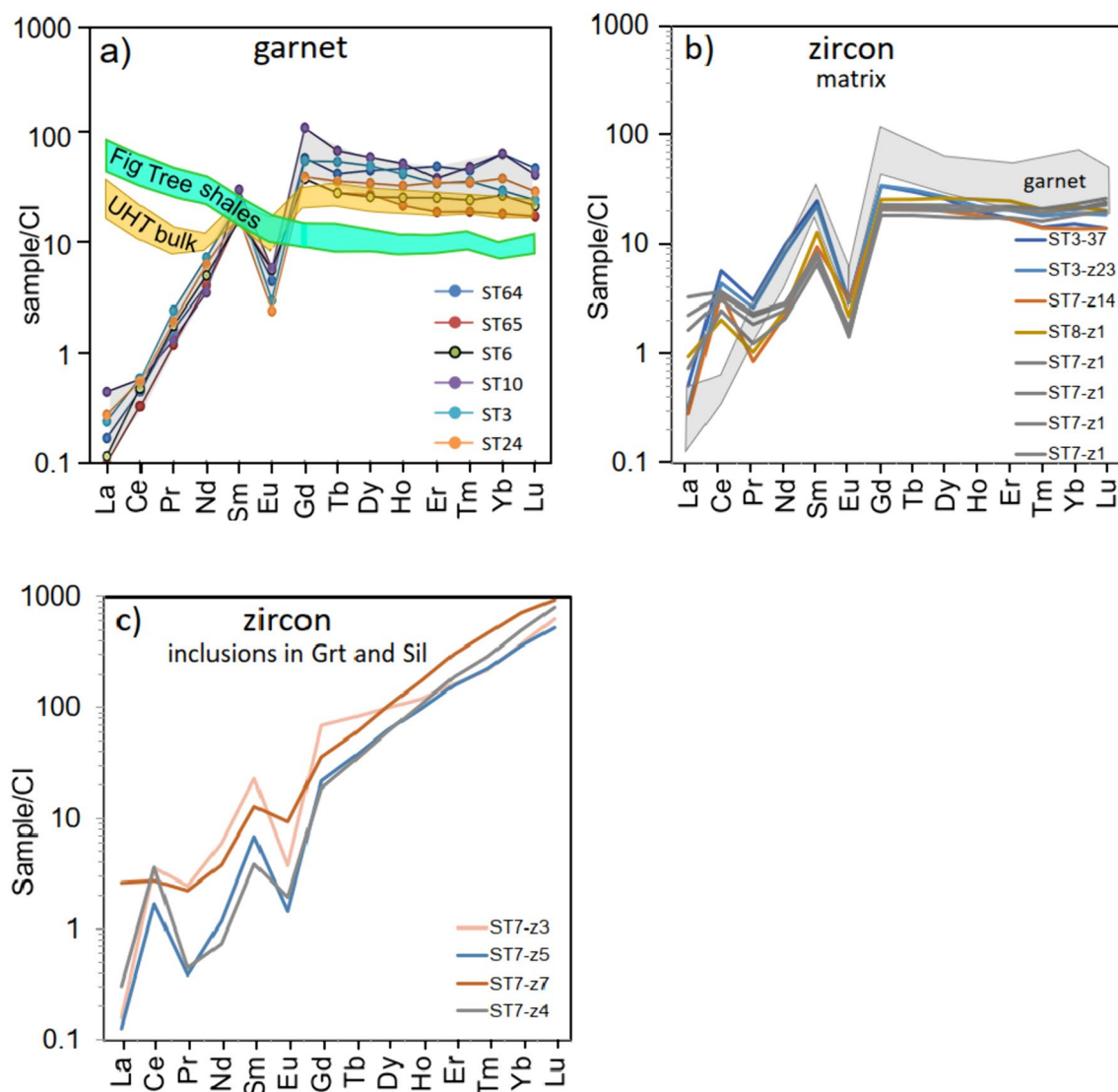


Fig. 7 **a** REE patterns of garnet from six UHT granulites from Star (normalized to McDonough and Sun 1995). They represent the whole range of garnet compositions found in Star UHT granulites. The range of UHT bulk rock compositions from Lace, Voorspoed and Star (yellow) is taken from Schmitz and Bowring (2003a) and of Fig Tree

shales (black) from Toulkeridis et al. (2015). **b** Composition of interstitial zircon grains (matrix) with flat middle to heavy REE patterns and negative Eu– and positive Ce anomalies. **c** Composition of zircon inclusions in garnet and sillimanite with steep middle to heavy REE patterns and negative Eu– and positive Ce-anomalies

displayed there as Tera-Wasserburg diagrams with outliers identified by dashed ellipses. Outliers were identified by eye and by the trace element contents of garnet (electronic Appendix Table AX). They may be caused by accidental co-ablation of U- or Pb-rich mineral inclusions, by contamination with kimberlite melt/fluid along cracks and rims or by the analysis of retrograde garnet. They were excluded from the regression line calculations. Inclusions of zircon or monazite are readily recognized as U, Th, or Pb spikes and high Zr and LREE in the U–Pb isotope data (Millonig et al. 2020) and contamination by kimberlite by elevated K, Rb, LREE and Sr concentrations. Data points for retrograde garnets fall to the right of the isochron. They are rare except

in sample ST14 where they form a second alignment (see Appendix Table A1, seq 2). Examples with few outliers are shown in Fig. 8a–d. An extreme case for the number of outliers is sample ST6 with high concentrations of K and Sr for each data point (Fig. A3). Excluding such data points, the age changes from 2918 ± 310 to 2993 ± 60 Ma and reduces the MSWD from 37 to 0.88.

In seven samples we analyzed both garnet and sillimanite (Table 3). Sillimanite is distinguished from coexisting garnet by its three times higher count rates for Al (Fig. 8e), a high proportion of Pb and lower abundances of most trace elements, including U (Fig. 8f). The low U/Pb ratio of sillimanite minimizes the ingrowth of radiogenic Pb, and therefore

Table 3 Compilation of garnet U–Pb lower intercept ages (2σ errors after Ludwig 2012 respectively Gerdes and Zeh (2006, 2009), initial $^{207}\text{Pb}/^{206}\text{Pb}$, MSWD values, number of used/measured analyses (n) and mean U and Pb contents

Sample	Age (Ma)	$(^{207}\text{Pb}/^{206}\text{Pb})_i$	MSWD	n used/all	U (ng/g) mean	Pb (ng/g) mean	Sil regr
ST2	2733 ± 37/46	1.0772 ± 0.0074	2.19	53/54	14.2	25.5	X
ST61	2769 ± 71/76	1.0098 ± 0.0278	3.2	39/55	4.1	16.2	
ST14 WAVG	2956 ± 46						
ST14 seq2	2924 ± 28/40	1.0580 ± 0.0259	1.0	53/60	3.3	8.2	
ST14 seq4	2988 ± 42/51	1.0399 ± 0.0180	2.07	41/56	4.1	11.1	
ST12	2942 ± 41/50	1.0823 ± 0.0080	2.19	49/59	1.7	4.4	X
ST8 Spr	3022 ± 27/41	1.0348 ± 0.0187	1.58	47/57	9.3	7.4	
ST3	2965 ± 24/38	1.0712 ± 0.015	1.43	51/60	12.5	13.6	X
ST9	2983 ± 67/73	1.0327 ± 0.0251	2.26	51/61	1.6	3.8	X
ST6 WAVG	3025 ± 79						
ST 6 seq2	2997 ± 54/61	1.0895 ± 0.0136	1.12	44/60	0.6	2.2	
ST6 seq4	3052 ± 93/98	1.0567 ± 0.0212	1.59	38/57	0.6	3.1	
ST10	3001 ± 37/47	1.0784 ± 0.002	0.87	54/60	1.9	24.7	X
ST63 Spr	3009 ± 74/80	1.0084 ± 0.0403	2.68	52/62	1.3	3.2	
ST5	3077 ± 67/74	0.9312 ± 0.0272	2.42	52/60	2.0	6.7	
ST65 Spr	3027 ± 98/103	0.8963 ± 0.0361	1.64	56/60	0.7	2.3	X
ST64	3096 ± 43/53	1.0678 ± 0.0220	1.68	59/60	2	6.8	
ST70	3096 ± 37/48	1.0567 ± 0.007	3.05	53/58	2.3	6.8	X
ST66	3097 ± 63/70	1.0165 ± 0.0273	2.18	53/53	0.7	1.7	
ST7 Spr	3133 ± 127/131	0.9584 ± 0.0265	1.62	54/57	0.6	2.5	

Regression calculations were done unanchored. Also given are weighted averaged ages (WAVG) for two doubly measured samples. All data and Tera-Wasserburg diagrams are given in Tables A1 in the electronic appendix

Spr = sapphirine present. X = both sillimanite and garnet isotope data have been used for age calculations

defines the initial $^{207}\text{Pb}/^{206}\text{Pb}$ ratio (i.e., the common-Pb component) during crystallization of the equilibrated metamorphic mineral assemblage. Sillimanite data points plot on the same regression line as garnet, but close to the y-axis of the Tera-Wasserburg diagram (Fig. 8 d and Table A1). A regression of sillimanite and garnet data from ST10 yielded an age of 3000 ± 38 Ma, similar to, but slightly more precise than an age of 2990 ± 42 Ma derived for garnet alone (Fig. 8d). Since sillimanite is synmetamorphic with garnet, the age derived from the combined data of both phases is preferred for such samples (Table 3).

Tiny rutile exsolution needles (see above “[Sample description](#)”) were identified optically in a number of garnet and quartz grains in this study as already described by Dawson and Smith (1987). However, we did not observe compositional spikes or outliers associated with rutile exsolution. The exsolutions are so small and evenly distributed that they are averaged out by the large-diameter laser beam. As the rutile needles were exsolved from the garnet, their chemical components (Zr, Si, Ti, U) must have been incorporated in the garnet structure at the time of peak metamorphism and co-exsolved during cooling (cf. Keller and Ague 2019). Due to the large laser beam diameter, these elements are reintegrated, and the obtained U–Pb date is interpreted to reflect

garnet growth prior to the exsolution of rutile upon cooling and decompression.

The lower intercept of the unanchored regression line with the Concordia defines the ages presented in Table 3 and Fig. 9. The individual uncertainties (2σ) vary between ± 1.0 and $\pm 2.6\%$ (± 20 – 80 million years), with one extreme of ± 130 million years for the oldest age (Table 3). The average of the uncertainties from the regression of U–Pb isotopic data calculated with Isoplot 4.15 (Ludwig 2012) is ± 57 million years, i.e., a relative uncertainty of approximately 2% (2σ). This is the same as that reported in earlier published LA-ICPMS U–Pb garnet geochronology studies with three orders of magnitude higher U contents (8000–35,000 ng/g; e.g. Wafform et al. 2018; Yang et al. 2018). Garnet in the present study contains < 30 ng/g, similar or lower than garnet in the study of Millonig et al. (2020).

Each sample displays a single date population, as evidenced by MSWDs mostly between one and two for each regression. While no intra-sample variability is observed, the obtained dates between samples span a wide range of nearly 400 million years from 3.10 to 2.75 Ga. Fourteen of the samples fall in the 210-million-years age range between 3.14 and 2.93 Ga, whereas only two samples give a date of ca. 2.72 Ga. A Kernel density estimation curve

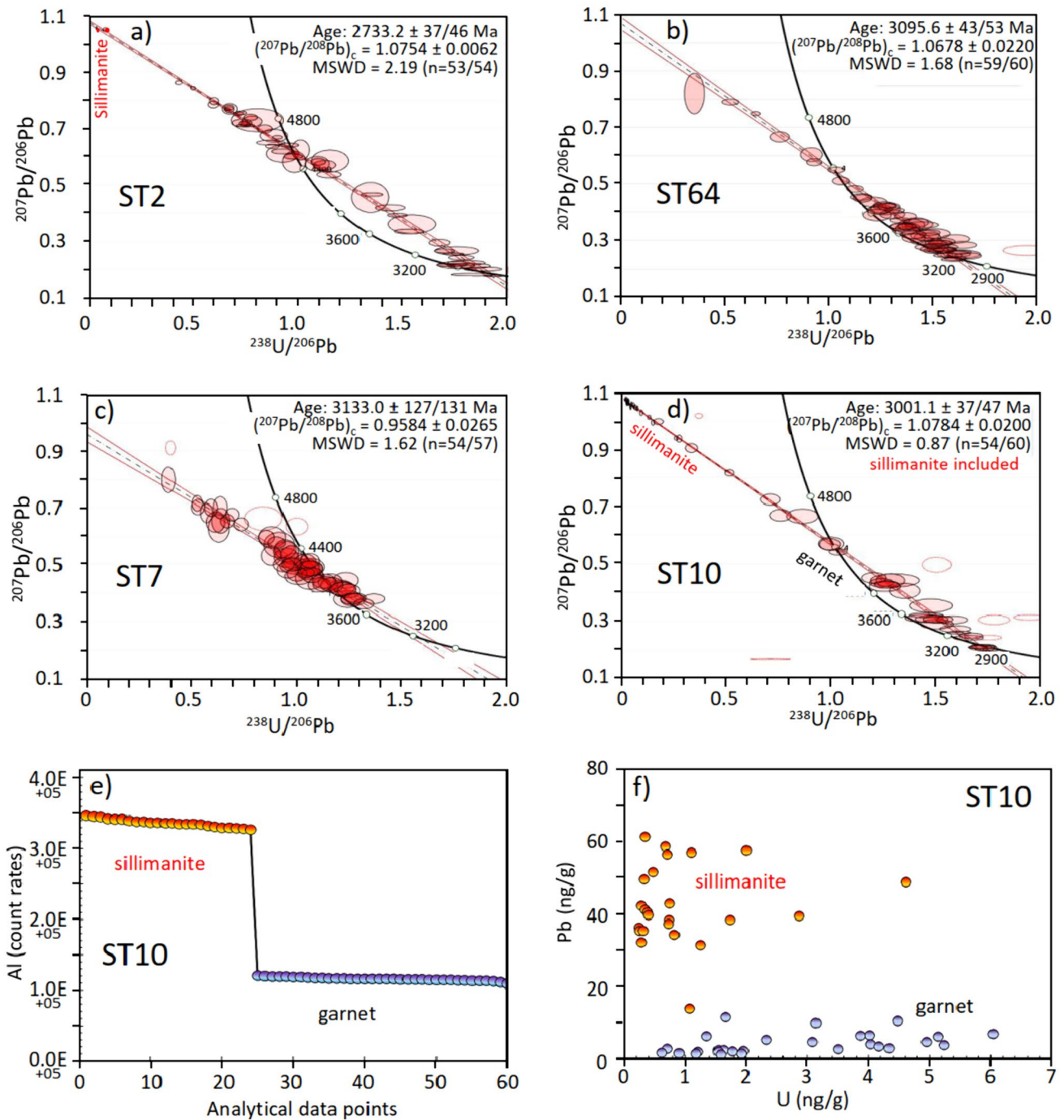


Fig. 8 Tera-Wasserburg diagrams with garnet U–Pb ages for samples ST2 (a), ST64 (b), ST7 (c), and ST10 (d). In a and d, U–Pb ages with and without sillimanite U–Pb data considered are shown. e Higher

count rates for Al distinguish sillimanite from garnet in the LASS data set. f sillimanite generally has higher Pb and lower U contents than garnet

(Vermeesch 2012) shows three peaks at 3.09, 3.01 and 2.75 Ga (Fig. 9a). The ages of the youngest samples ST2 and ST61 are indistinguishable from the zircon ages determined by Schmitz and Bowring (2003a) and from our own U–Pb ages by LA-ICPMS (see below).

Zircon U–Pb ages

U–Pb ages were determined via LASS-ICPMS) from intergranular zircons and from zircon inclusions in garnet and sillimanite from three samples (ST3, ST7, ST8). The

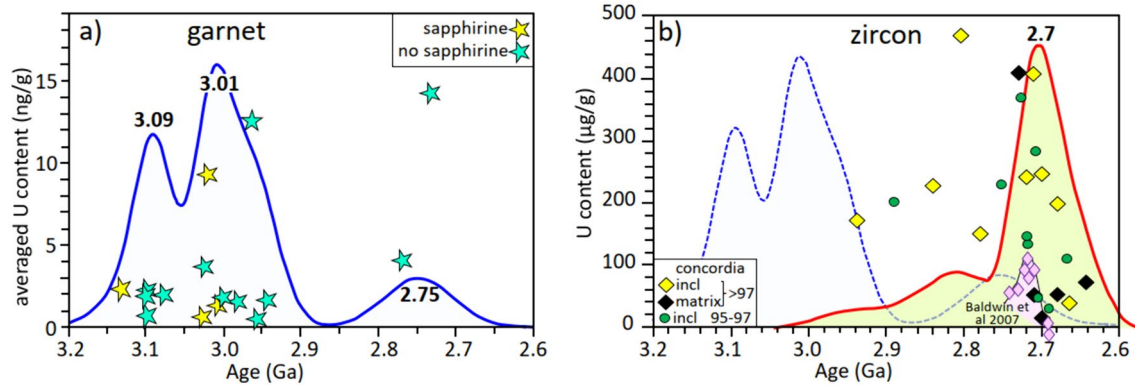


Fig. 9 **a** Averaged U content of garnets vs their U–Pb age with a Kernel density estimation curve for garnet ages (Vermeesch 2012). **b** Uranium content of zircon from samples ST3, ST7 and ST8 plotted against $^{207}\text{Pb}/^{206}\text{Pb}$ ages. Black diamonds are matrix grains and both yellow diamonds and green dots are inclusions (incl) in garnet and sillimanite. Green dots are analyses with 95–97% concordance, the yellow and black diamonds represent analyses that are >97% con-

cordant. Ages fall mainly between 2.74 and 2.66 Ga but ages up to 2.94 Ga exist. The peak around 2.7 Ga coincides with the peak of zircon ages (their Type 2) determined Baldwin et al. (2007; violet field and diamonds) and interpreted as representing peak metamorphism. This age coincides with the youngest maximum of the garnet age-distribution curve

analytical results, ages and Wetherill diagrams are given in the appendix in Table A2. In Fig. 9b U concentrations of single spot analyses are plotted against lead-lead ages ($^{207}\text{Pb}/^{206}\text{Pb}$). We distinguish in Fig. 9b between ages with a Concordia agreement of 97–101% and 95–97% (Table A2) and between matrix and inclusion zircon grains. Ages range from 2938 ± 15 to 2640 ± 15 Ma with the majority around 2.71 Ga, the main peak in Fig. 9b. The ages overlap with the results of Schmitz and Bowring (2003a). All matrix zircon plot at the lower end of the observed age range. Four zircon grains, included in garnet or sillimanite, have significantly higher U–Pb ages up to 2938 Ma. The oldest zircon analysis agrees within uncertainty with the second-oldest peak of the garnet age distribution curve (Fig. 9b). Note, however, that most garnet analyses show ages as old or older than the oldest zircon age (Fig. 9). One analysis of a zircon grain intergrown with rutile gives a near-concordant age of only 1.34 Ga (not shown; Table A2).

Geothermobarometry

The mineralogical composition and petrologic appearance of the sapphirine-free and sapphirine-bearing granulites are very similar to the UHT granulite xenoliths described from Lace by Dawson and Smith (1987) and Dawson et al. (1997). The latter authors presented a field of peak metamorphism for coexisting garnet, sapphirine and quartz for the FMAS (FeO–MgO–Al₂O₃–SiO₂) system based on evaluations of Bertrand et al. (1991) and Hensen and Green (1973). Their fields are reproduced in the electronic appendix in Fig. A1. Accordingly, peak metamorphism must have reached conditions of $T > 1050$ °C and P between 1.0 and 1.3 GPa or $T > 1030$ °C and P of 0.8–1.1 GPa. We calculated pressures

from the grossular and anorthite contents of coexisting garnet and plagioclase, respectively, at 1050 and 1100 °C using the garnet-alumosilicate-quartz-plagioclase (GASP) barometer of Hodges and Crowley (1985) as implemented in Program GTB (Spear et al. 1991). The results are shown for two different temperatures in Fig. 10a in a diagram of pressure versus $X_{\text{Ca}}^{\text{Grt}}/\text{An}^{\text{pl}}$, the critical pressure-determining variable and given in Table 4. Pressures range from 0.88 to 1.15 at 1050 °C and from 0.95 to 1.21 GPa at 1100 °C. Only sample ST2 gives much higher pressures with 1.33 and 1.40 GPa, respectively. Pressures calculated from the few samples with higher CaO at garnet rims are elevated at a constant temperature. Consistent with the deductions by Dawson et al. (1997) for Lace, we interpret this as the result of isobaric cooling.

Pressures calculated at 1100 °C are plotted in Fig. 10b against age. The oldest sample (ST7, 3141 ± 127 Ma) lacks plagioclase and the pressure cannot be determined. The pressure range of the two age groups with peaks at 3.09 and 3.01 Ga is very similar, and no age-dependent pressure variation is apparent. The typical 2σ uncertainties on the GASP barometer, including calibration uncertainty and propagated uncertainties in the temperature, are ± 0.2 GPa and our P data largely fall within 1.1 ± 0.2 GPa. Thus, small P differences may exist between samples that cannot be resolved within uncertainty.

Ti-in-zircon temperatures (Watson et al. 2006) in samples from Star fall into two groups with estimates that range between 939 and 1074 °C with a median at 1039 °C and 824–885 °C (Fig. 11). The highest temperatures exceed those given by Baldwin et al. (2007) but there is overlap at the lower temperatures. The highest temperatures record temperatures close to or at the conditions estimated for

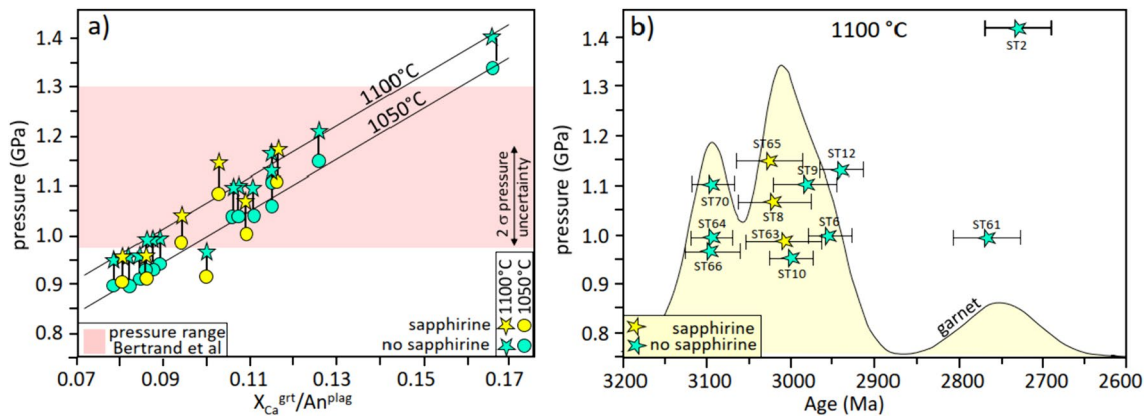


Fig. 10 **a** Pressures for UHT granulites calculated with the GASP barometer using the calibration of Hodges and Crowley (1985) from coexisting garnet and plagioclase in the presence of sillimanite and quartz at 1050 and 1100 °C. The change of 50°C causes an increase of apparent pressure of approximately 0.06 GPa (i.e. 1.2 MPa/K). No pressure estimate is available for ST7, because this sample lacks

plagioclase. The red field indicates the pressure range for UHT metamorphism as suggested by Bertrand et al. (1991). **b** Calculated pressure plotted against age. The pressure ranges for the two age groups at around 3.10 and 3.0 Ga overlap, and there is no age-dependent pressure variation

Table 4 Pressures (in GPa) calculated with the GASP geobarometer for 1050 and 1100 °C

Sample	ST4	ST8	ST65	ST68	ST69	ST1	ST2	ST6	ST10	ST58
1050 °C	0.98	1.01	1.08	1.12	0.90	1.15	1.34	0.94	0.90	0.90
1100 °C	10.4	1.07	1.15	1.18	0.96	1.22	1.42	1.00	0.95	0.96
Sample	ST59	ST62	ST64	ST71	ST12	ST63	ST61	ST70	ST66	ST9
1050 °C	1.11	1.04	0.93	0.95	1.06	0.92	0.92	1.04	0.91	1.04
1100 °C	1.17	1.11	0.99	1.00	1.13	0.98	0.99	1.10	0.97	1.10

the stability of garnet, sapphirine and quartz. By contrast, Zr-in-rutile temperatures (Ferry and Watson 2007) from rutile exsolutions and inclusions in garnet show temperatures between 800 and 900 °C and are even lower, down to 600–700 °C, in matrix rutile grains. We did not use a thermometer with a pressure correction because our rocks were metamorphosed in the same pressure range as the experiments (i.e. $P = 1.0$ GPa; Watson et al. 2006). Zirconium diffusion in rutile is sufficiently fast such that the matrix rutiles can adjust to lower temperatures upon cooling (Cherniak et al. 2007; Pape et al. 2016; Dohmen et al. 2019). The Zr-in-rutile temperatures recorded in our samples are at the lower end of temperature estimates from other UHT granulites (Harley 2016). When rutile grains become isolated from an external Zr sink (i.e. zircon) upon cooling they cannot, or only partially adjust to the lower temperatures (Taylor-Jones and Powell 2015). This may apply to rutile inclusions and exsolutions in garnet that preserve the Zr contents equilibrated at higher temperatures (e.g., Zack et al. 2004; Pauly et al. 2016).

Lowest temperatures are recorded by pentlandite exsolutions in monosulfides. Crystallization of pentlandite in the

Fe–Ni–S system is from about 550 °C downwards (Kitakaze et al. 2011; Firdu and Taskinen 2010) which suggests that the rocks cooled down to at least that temperature (Fig. 6a). These low temperatures are close to the present day temperatures of the lower crust as indicated from the extension of conductive geothermal gradients of the Kaapvaal craton (e.g. Bell et al. 2003). Monosulfides contain only small amounts of pentlandite and chalcopyrite exsolutions so that their measured composition is close to that from high temperatures. Therefore, monosulfide appears to be the only, single-phased sulfide at the conditions of UHT metamorphism. Its composition lies in the field of residual monosulfide within the extensive melt field at 1100 °C in the intermediate portion of the Fe–Ni–S system (Fig. 6b). Because of this compositional overlap we consider monosulfide as residual phase or immiscible liquid of partial melting of more complex sulfides.

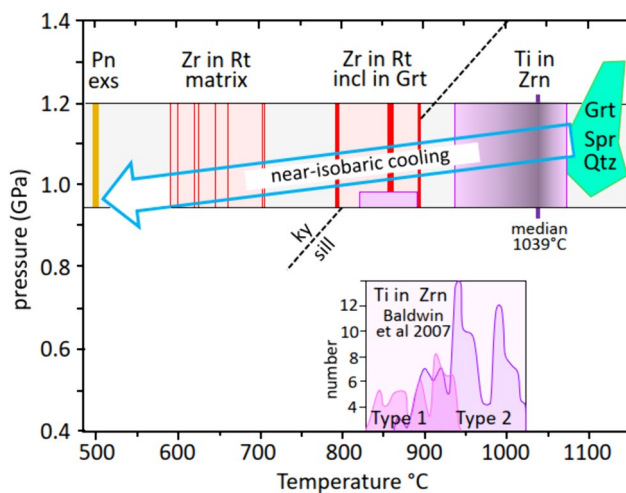


Fig. 11 Temperatures of zircon and rutile calculated with the single-grain Ti-in-zircon and Zr-in-rutile thermometers of Watson et al. (2006) and Ferry and Watson (2007), respectively. Temperatures in zircon range from 939–1074 to 824–885 °C for our EPMA measurements. Ti-in-zircon temperatures for the Lace and Voorspoed zircons range from about 830–1030 °C (Baldwin et al. 2007). Zr-in-rutile temperatures for rutile inclusions and exsolutions in garnet range from 800–900 °C and for rutiles in the matrix from 600–700 °C. The pentlandite exsolutions in monosulfide grains indicate the lowest temperatures around 500 °C (temperature by comparison with phase diagram, Fig. 6b). The grey band in the back denotes the GASP pressures calculated for 1100 °C in this study. The green field is the field for coexisting garnet, sapphirine and quartz after Dawson et al. (1997)

Discussion

The mineral assembly of the UHT granulites and their composition indicate that bulk rocks are high in MgO, FeO and Al₂O₃, low in Na₂O and CaO, barren in K₂O, and generally low in many incompatible elements, including the LREE (Dawson and Smith 1987; Schmitz et al. 2003a; this work). These geochemical features, together with strongly suprachondritic bulk-rock ¹⁴⁴Nd/¹⁴³Nd isotope ratios, led Schmitz et al. (2003a) to suggest that the UHT granulites are restites of partial melting of a sedimentary protolith with garnet as the main residual phase. Consistently, garnet has depleted LREE patterns, whereas the LREE appear to be elevated in the bulk rocks (Schmitz and Bowring 2003a). There is no phase with elevated LREE in sufficient abundance in the UHT granulites granulites to account for this enrichment. Our interpretation is that the elevated bulk-rock La–Ce–Pr contents are secondary and due to contamination by the kimberlite host magma as commonly observed in xenoliths (e.g. Jacob et al. 2005; Barth et al. 2001). High Cr and Ni contents in sapphirine, spinel (Spl), sillimanite and rutile (Dawson et al. 1997; see also “Results” above) suggest a high mafic to ultramafic component in a sedimentary precursor. The signature of a high Cr and Ni component is characteristic of pelites derived from the erosion of greenstone

belts (McLennan et al. 1983). Shales like the Archean Fig Tree shales from the Barberton greenstone belt are possible protoliths. Extensive partial melting at high pressures proceeded mainly in the presence of garnet (see also Schmitz and Bowring 2003a). Melts are successively generated by the breakdown of muscovite, biotite and K-feldspar with continuous removal of melt. This way, the residue becomes depleted in volatiles, whereas garnet increases in abundance as a peritectic and residual phase. Sulfides change accordingly, to become eventually monosulfide at peak metamorphic conditions either as a residual phase or a residual immiscible melt (see Fig. 6). An origin from the lower crust with temperatures above 1050 °C was derived by Dawson et al. (1997) from petrogenetic grids. These authors also deduced near isobaric cooling from thermobarometry. An origin from the lower crust is confirmed by our calculations with the GASP barometer that gave pressures between 0.9 and 1.1 GPa. There is no apparent correlation of pressure with age but the garnet age distribution curve allows the division into three age groups (Figs. 9 and 10).

There are two main age groups at around 3.1 and 3.0 Ga and a third, less pronounced, at 2.75 Ga. The older garnet spans a range of approximately 200 million years from 3.14 to 2.93 Ga. This age period could be interpreted to reflect UHT metamorphism that lasted for over 200 million years. This is supported by the long period of granitic magmatism in combination with basaltic volcanism of the Dominion group (Fig. 12). Alternatively, based on the maxima in the age distribution curve (Fig. 9a), two periods of UHT metamorphism may have occurred at around 3.1 and 3.0 Ga, separated by a period of cooling. Two periods are supported by the restricted age range of mid crustal granulites from the Vredefort dome and from Swaziland at 3.1 Ga by the culmination of intrusion ages of K-granites around that time (Kamo and Davis 1994; Pujol et al. 2003) and by a longer time lag until the onset of Dominion Group volcanism (2.99 Ga). Granulite terrains worldwide record short- and long-lived UHT metamorphism. Most are short-lived with several tens of million years. An example for long-lived UHT-metamorphism is documented from the Eastern Ghats Province of India with at least 80 million and possibly up to 200 million years from 1130 to 930 Ma (Korhonen et al. 2013). Another case is the late Archaean Napier Complex of East Antarctica where conditions of 950–1050 °C and 0.7–1.1 GPa were maintained for 135 million years (e.g., Ellis 1987; Horie et al. 2012; Suzuki et al. 2006; Harley 2016; Clark et al. 2018). Causes for UHT metamorphism include a thickened crust with elevated heat production from high contents of radioactive elements or an increased thermal flux from the underlying mantle (see overviews by Kelsey and Hand 2015 and Harley 2016). Specifically, Harley (2016) favors the concept of ultrahot orogens that was introduced by Chardon et al. (2009). Ultrahot orogens

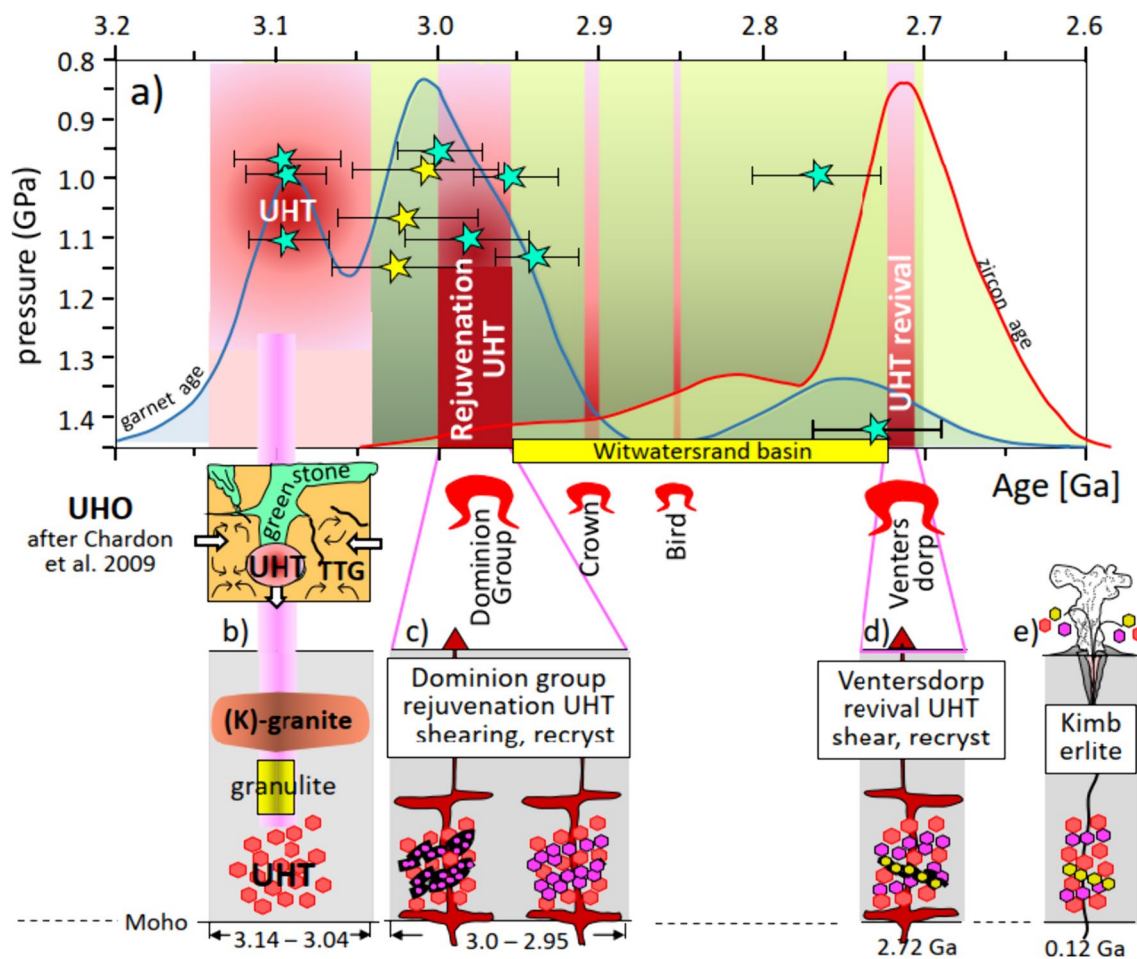


Fig. 12 **a** Pressure plotted against age. Garnet ages with error bars are shown as stars with an enveloping age distribution curve and zircon ages as an age distribution curve only. The vertical red bars give the age range for K-granites and mid-crustal granulite terrains, for the Dominion Group volcanism, the Crown and Bird basalts and for the Ventersdorp flood basalts. Shown underneath is a schematic diagram for the origin of UHT granulites in an ultrahot orogen setting and uprising diapirs to indicate various periods of basaltic volcanism. **b** Establishment of UHT conditions indicated as red hexagons, contemporaneous generation of mid-crustal granulites (Vredefort dome,

Swaziland) and crustal melting with generation of K-rich magmas. The dark-shaded center of the vertical bar indicates the most prominent ages of K-granites and granulites. **c** Second garnet generation around 3.0 Ga through rejuvenation of UHT conditions by Dominion-Group magmatism accompanied by shearing and recrystallization of shear zones (curved black lines and pink hexagons). **d** Renewal of UHT conditions by Ventersdorp flood basalt volcanism, shearing and recrystallization (yellow hexagons). **e** Eruption of Star kimberlites that sampled xenoliths including all three garnet generations

develop on hot, weak lithosphere whereby higher mantle potential temperature (T_p) and higher heat production in the Archean crust-lithosphere system provide favorable conditions. These orogens are characterized by rapid accretionary crustal growth, thickening by downward movements of supracrustal units (sagduction), diapirism, juvenile magmatism and high geothermal gradients (Gapais et al. 2009).

The older U–Pb ages of Star-UHT-xenoliths were preserved in most garnet samples despite the third, albeit short-lived crustal UHT revival at 2.72 Ga (Fig. 12). This suggests a very high closure temperature of the U–Pb system in garnet, in excess of 1050–1100 °C. If so, garnet has the capacity to retain old ages even under temperature conditions at the most extreme end of crustal metamorphism. This opens

the possibility for an evaluation of the long-term thermal evolution of the lower crust of the Kaapvaal Craton. The period around 2.72 Ga is documented by a maximum in the garnet age distribution curve and by zircon ages from Bowring and Schmitz (2003a) and from this study. The latter authors attributed this youngest period to the Ventersdorp flood basalts at 2714 ± 8 Ma (Armstrong et al. 1991) as the main cause for short-lived (5–10 million years) UHT metamorphism. We interpret the youngest groups of garnet and the main group of zircon ages to reflect a reestablishment of UHT conditions by the Ventersdorp magmatism. Zircon from our study spans a wider age range than reported by Schmitz and Bowring (Fig. 9b). Some are slightly younger and others are older reaching up to 2.94 Ga overlapping

with the second garnet age group. Equilibrium between garnet and zircon can be tested from the partitioning of REE (Rubatto 2002; Rubatto and Hermann 2007 and Taylor et al. 2015). Garnet patterns are fairly uniform with flat middle to heavy REE whereas zircon REE patterns are twofold: one group with flat middle to heavy REE patterns, the other with positively sloping REE (Fig. 7). Zircon and garnet with flat HREE yield partition coefficients below unity for middle to heavy REE, that overlap with the experimental results reported by the above authors mentioned for temperatures between 900 and 1000 °C. They thus indicate equilibrium between garnet and zircon. Zircons with positively-sloping HREE are not in equilibrium with garnet and apparently preserve an earlier growth stage at lower temperatures.

Garnet age groups are set in relation to events in crust and mantle in Fig. 12. The oldest garnet age group with a peak around 3.1 Ga ties in with the widespread intrusion of granitic magmas on the Witwatersrand block between 3.14 and 3.04 Ga. It also coincides with the time of granulite metamorphism at mid-crust levels of Swaziland and the Vredefort dome (Fig. 12b). Of note, the Vredefort dome lies in the extension of the alignment of the UHT-xenolith-bearing kimberlites along the NNE axis of the Witwatersrand basin (Fig. 1). Granitic magmatism, mid-crustal granulite facies metamorphism and lower crust UHT granulite xenoliths may be the witnesses of ultra-hot orogen(s) that developed in the wake of the assembly of the Witwatersrand block at 3.2 Ga from three terrains (Fig. 1; see also Schoene et al. 2008). The high-temperature conditions in the lower crust around 3.1 Ga were likely based on a high mantle potential temperature (T_p) in the Archean (1500–1600 °C; Herzberg et al. 2010) and internal heat production from radioactive elements. These elements may reside in (metamorphosed) TTGs and in subducted/sagducted sedimentary protoliths of the UHT granulites and the source of crust-derived granites (see also Marschall et al. 2010). The isotope and trace element composition of the UHT granulite xenoliths suggest a sedimentary origin (Schmitz and Bowring 2003a) with a composition similar to the Barberton shales. Barberton shales are high in K, U and Th and have, on average, approximately 3.6 wt% K_2O , 1.7 $\mu\text{g/g}$ U and 5.4 $\mu\text{g/g}$ Th (Toulkeridis et al. 2015). Today's heat production from these elements is approximately $= 1.01 \mu\text{Wm}^{-3}$ (calculated after Rybach 1988; see also Kramers et al. 2001). The higher radiogenic heat production in the Archean increases this estimate to $2.85 \mu\text{Wm}^{-3}$ at 3.1 Ga, which is approximately 8 times higher than the heat production in the present-day average lower continental crust.

Based on our data and data from the literature, we suggest the following model for the temporal evolution of the lowermost crust of the Kaapval craton. At ca 3.10 Ga, metamorphism at mid-crustal levels now exposed in the Vredefort Dome reached ca. 900 °C. Temperatures were higher at

greater depths and presumably rose above 1050 °C at 30–40 km depth. The UHT assemblage of garnet + sapphirine + sillimanite + quartz was established at that time as a consequence of the transfer of the K–Th–U-rich sedimentary protoliths to lower crust depths. This process was accompanied by heating and substantial partial melting below and above the stability of hydrous silicates to the extent of consumption of K-feldspar (Brown and Kohonen 2009).

The first UHT event at approximately 3.1 Ga may have been followed by a period of cooling until renewed heat input from the mantle into the crust occurred at 3.00–2.95 Ga, as indicated by the basaltic volcanism of the Dominion Group at this time. Heat may be transferred by advection via melt channels or by conduction. Transfer via melt channels is localized and short-lived so that mineral assemblages and compositions would only partially equilibrate. In contrast, heat transfer via conduction is regional, long lasting and ensures time for compositional adjustment and equilibration. It was apparently not sufficient to disturb or re-equilibrate the U–Pb system in garnet, because of an exceedingly high closure temperature of this system in garnet (presumably higher than 1100 °C) as indicated by the preservation of 3.1 Ga garnet during subsequent UHT metamorphism.

However, not all samples yielded garnet U–Pb ages that record the oldest metamorphic event at approximately 3.1 Ga. Instead, there is also a garnet age group with a peak at approximately 3.0 Ga. It overlaps with the intrusion and extrusion of the magmatic members of the Dominion Group between 2.99 and 2.96 Ga (Fig. 12a). The age of the intrusive and extrusive emplacement of the mafic and felsic magmas at the base of the Witwatersrand Basin was originally determined as 3.07 Ga (Armstrong et al. 1991; Agangi et al. 2020). However, Paprika et al. (2021) showed that these older dates stem from xenocrystic zircons and that, instead, magmatic zircons from the felsic and mafic members yield ages of 2.99 Ga, and 2.96 Ga respectively. Also, zircon from the lowermost sediments of the Witwatersrand Basin records a maximum age of 2.99 Ga. The heat input renewed UHT conditions and reset a subset of the garnet dates. There are two mechanisms by which garnet dates may have been reset: Pb diffusion and recrystallization. The closure temperature for thermally activated diffusion in a crystal lattice depends on temperature, cooling rate, and grain size (Dodson 1973), where large grains and fast cooling rates result in higher closure temperatures. If Pb diffusion would be responsible for resetting garnet dates to 3.0 Ga (or 2.72 Ga in even younger samples), we would anticipate significant scatter in Tera Wasserburg space as a function of grain size and position of analysis (e.g. garnet core vs rim). Yet, the U–Pb data for each sample can be fit with a single well-defined regression line (Fig. 8), which is inconsistent with Pb diffusion. Alternatively, some samples may have experienced renewed UHT metamorphism and Pb diffusion

would be very rapid, such that a given xenolith would be fully reset to reach homogeneity. However, if all xenoliths are sampled from similar depths in the crust, as suggested by our pressure calculations, it is unlikely that only some samples would be locally reset by thermal diffusion. Based on these constraints, we instead propose that garnet ages at approximately 3.0 Ga represent heterogeneous recrystallization in different segments of the deep crust. Our suggested solution is shown in a sketch in Fig. 12c: Dominion group magmatism was accompanied by shearing, (ultra)mylonitisation, and possibly renewed partial melting in the lower crust. These shear zones perhaps focused on domains in the crust in which some hydrous minerals survived metamorphism at 3.10 Ga, garnet was newly formed in these mylonite zones and recrystallized at the prevailing high temperatures. While our samples do not show evidence of shearing or grain size reduction, this could be explained by the high temperatures at UHT conditions that would enable fast recrystallization of the rock fabric. Many samples exhibit a second generation of thin garnet overgrowths which extend from larger garnet porphyroblasts (Fig. 2c). While these garnet overgrowths (which occur along the grain boundaries between quartz, sapphirine, and plagioclase) are too small for LA-ICP-MS analysis, these textures are consistent with multi-stage garnet growth.

We interpret the recrystallized garnet date around 3 Ga to document a thermal perturbation in the crust as a result of Dominion group volcanism. Temperatures remained high in the crust during continued subsidence of the Witwatersrand Basin with the deposition of predominantly marine sediments of the West Rand Group and renewed small-volume basaltic volcanism (Crown and Bird lavas) at the time of the collision of the Witwatersrand and Kimberley blocks (2.9 Ga). Approximately 150 million years of relative quiescence followed, during which the Witwatersrand Basin deepened further by more than 2 km (estimated from the 2.9 km thick Central Rand Group with the Bird lavas at its base; Coward et al. 1995). A major tectonomagmatic event affected the central and southwestern Kaapvaal Craton a third time with the emplacement of the Ventersdorp flood basalts at around 2.72 Ga, which covered an area of approximately 300,000 km² (Armstrong et al. 1991; Van der Westhuizen et al. 1991). This event caused a renewed thermal impact onto the lower crust, shearing and recrystallization that is recorded in zircon in the UHT granulites and by garnet in samples ST2 and ST61 (Schmitz and Bowring 2003a; this study).

This model explains the repeated ultrahigh temperature periods as documented in garnet. However, zircon may tell a different story. All zircon grains in the study of Schmitz and Bowring (2003a) yielded ages of around 2.72 Ga (Fig. 12), with no record of the older events. Zircon occurs as intergranular grains in the UHT rocks and as inclusions in all

metamorphic minerals (Schmitz and Brown 2003a). We also found larger, intergranular zircon grains and smaller, roundish zircon grains included in garnet and sillimanite (Fig. 3). This suggests that zircon existed before the growth of garnet but may have also grown at a late stage, postdating the formation of the rock-forming minerals. Zirconium can be incorporated in garnet and rutile at very high temperatures (see Introduction), such that intergranular zircon probably grew below peak metamorphic temperatures at the onset of cooling. Also, temperatures of UHT metamorphism are above the closure temperature for the U–Pb system in zircon (Mezger et al. 1989; Dahl 1997). Zircon is thus expected to grow only during cooling and/or yield young ages because zircon can adjust by U–Pb by diffusion down to its closure temperature. In either case, zircon would not record the time of peak metamorphism. Schmitz and Bowring (2003a) determined the age of single grain separates and possibly missed small inclusions in garnet and sillimanite. They would have thus been biased to zircon grains that formed at a late stage at the onset of cooling following the youngest UHT event. In contrast, zircon inclusions in garnet and sillimanite may yield older ages due to shielding by the host mineral. We tested this by in-situ U–Pb dating using split-stream LA-ICPMS. We mostly found ages around 2.7 Ga, confirming the results of Schmitz and Bowring (2003a). However, four zircon inclusions revealed older ages of up to 2.94 Ga. The full range of zircon ages is displayed in Figs. 9b and 12. The oldest zircon is indistinguishable from the second maximum in the garnet age distribution curve at 2.96 Ga (Figs. 9b and 12). Our new findings confirm the dominating role of the Ventersdorp flood basalts in resetting the majority of zircon to an age of approximately 2.72 Ga, as advocated by Schmitz and Bowring (2003a). However, that event did not entirely erase the record of zircon inclusions in garnet and sillimanite and neither did it reset the older ages recorded in garnet.

Conclusions

We obtained a date range for garnet from approximately 3.1–2.7 Ga with three peaks at 3.09 Ga, 3.01 Ga and 2.75 Ga. In contrast, zircon U–Pb dates from this and previous studies show a single dominant age peak at 2.72 Ga. Few older dates of up to 2.94 Ga are recorded by zircon grains included in garnet and sillimanite. Our results demonstrate that garnet can retain U–Pb dates throughout younger UHT metamorphic events in granulites, where zircon is reset by Pb loss or records late exsolution, likely from rutile and garnet. Inclusions of zircon in sillimanite or garnet may be partially shielded from age resetting and in some cases also provide a record of older metamorphic events. Despite similar pressure conditions deep in the crust, garnets from each xenolith yield a single well-defined date. These data

are inconsistent with diffusional resetting of the U–Pb system in garnet and likely reflect selective metamorphism, deformation, recrystallization, and annealing of different portions of the lower Kaapvaal crust. These data suggest that the closure temperature for the U–Pb system in garnet is in excess of the UHT conditions that prevailed again for the sapphirine-quartz-bearing granulites at 2.96 Ga and at 2.72 Ga. This observation leads us to conclude that garnet U–Pb geochronology can record the most extreme conditions of crustal metamorphism, which may not be recorded by other geochronometers.

The garnet ages presented here also show that very high temperatures existed already very early on in the history of the Kaapvaal craton. Initially, high temperatures at 3.1 Ga were likely caused by crustal internal incubation due to the deep-crustal burial of sediments rich in heat-producing elements. Later events saw periods of advective heat input from the underlying mantle by magmas of the Dominion Group volcanic succession between 2.99 and 2.90 Ga and of the Ventersdorp flood basalts at around 2.72 Ga. These events caused a rejuvenation of UHT conditions in the Kaapvaal lower crust.

The extremely high temperatures of UHT metamorphism in the lower crust at around 3.1 Ga run converse to the conception that a cold thick mantle lithosphere is formed at around this time. This concept is based on previous Sm–Nd and Re–Os ages of diamonds and mantle xenoliths (e.g. Richardson et al. 1984; Pearson and Wittig 2008). Formation of a thick lithosphere around that time was already considered as unlikely e.g. by Moser et al. (2001), Schmitz and Bowring (2003a), Schoene et al. (2008) and Marschall et al. (2010). Their counterarguments are the generation of granitic magmas and granulite metamorphism at around 3.1 Ga. Heat generation was within the crust from the radioactive inventory since oxygen isotopes of zircons in the granites do show mainly crustal values (Marschall et al. 2010). UHT conditions in the lower crust at around 3.1 Ga rule out the establishment of a cool thick lithosphere even more so. They may even be witnesses of relamination processes as far back in time (Hacker et al. 2011). The two arguments from Re–Os and diamond ages are not directly applicable as proof for the establishment of lithosphere at least not for the Witwatersrand block. Old diamond ages are only reported from the Kimberley block (Richardson et al. 1984) and not from the Witwatersrand block and only three T_{RD} ages > 3.0 Ga are reported from the Witwatersrand block (Carlson and Moore 2004). They determined a maximum at 2.9 Ga that is entirely in agreement with the maximum of our own nine unpublished data on Re–Os from spinel peridotites underneath Star. Our new U–Pb data of UHT-metamorphism in the lower crust necessitate a time younger than 3.1 Ga the formation of a cool stable lithosphere.

We were able to determine U–Pb dates from garnet crystals with extremely low U concentrations of less than 15 ng/g. The in-situ age determination on a major phase with such low concentrations of U opens wide possibilities to put new constraints on the evolutionary history of the lower crust, the upper mantle and of metamorphic systems in general.

Supplementary Information The online version contains supplementary material available at <https://doi.org/10.1007/s00410-024-02121-4>.

Acknowledgements We thank Nils Prawitz and Martin von Dollen for preparation of polished thin sections and mounts. We also thank the editor Dante Canil and the two reviewers Jesse Reimink and Francisco Apen for their thoughtful reviews and helpful suggestions. This is FIERCE contribution No. 156.

Funding Open Access funding enabled and organized by Projekt DEAL. This work was supported by the Deutsche Forschungsgemeinschaft (MA 5366/3–1) and the Hundred-Talent Program of China (Chinese Academy of Sciences; Y8CR001000). FIERCE is financially supported by the Wilhelm and Else Heraeus Foundation and by the Deutsche Forschungsgemeinschaft (DFG: INST 161/921-1 FUGG, INST 161/923-1 FUGG and INST 161/1073-1 FUGG).

Data availability All data are available in the electronic appendix.

Open Access This article is licensed under a Creative Commons Attribution 4.0 International License, which permits use, sharing, adaptation, distribution and reproduction in any medium or format, as long as you give appropriate credit to the original author(s) and the source, provide a link to the Creative Commons licence, and indicate if changes were made. The images or other third party material in this article are included in the article's Creative Commons licence, unless indicated otherwise in a credit line to the material. If material is not included in the article's Creative Commons licence and your intended use is not permitted by statutory regulation or exceeds the permitted use, you will need to obtain permission directly from the copyright holder. To view a copy of this licence, visit <http://creativecommons.org/licenses/by/4.0/>.

References

- Agangi A, Hofmann A, Hegner E, Xie H, Teschner C, Slabunov A, Svetov SA (2020) The Mesoarchaean Dominion Group and the onset of intracontinental volcanism on the Kaapvaal craton—geological, geochemical and temporal constraints. *Gondwana Res* 84:131–150
- Altermann W, Hålbich IW (1991) Structural history of the southwestern corner of the Kaapvaal Craton and the adjacent Namaqua realm: new observations and a reappraisal. *Precambr Res* 52:133–166
- Armstrong RA, Compston W, Retief EA, Williams IS, Welke HJ (1991) Zircon ion microprobe studies bearing on the age and evolution of the Witwatersrand triad. *Precambr Res* 53:243–266
- Baldwin JA, Brown M, Schmitz MD (2007) First application of titanium-in-zircon thermometry to ultrahigh-temperature metamorphism. *Geology* 35(4):295–298
- Barth MG, Rudnick RL, Horn I, McDonough WF, Spicuzza MJ, Valley JW, Haggerty SE (2001) Geochemistry of xenolithic eclogites from West Africa, part I: a link between low MgO

- eclogites and Archean crust formation. *Geochim Cosmochim Acta* 65(9):1499–1527
- Baxter E, Scherer E (2013) Garnet geochronology: timekeeper of tectonometamorphic processes. *Elements* 9:433–438. <https://doi.org/10.2113/gselements.9.6.433>
- Bell DR, Schmitz MD, Janney PE (2003) Mesozoic thermal evolution of the southern African mantle lithosphere. *Lithos* 71(2–4):273–287
- Beranoaguirre A, Vasiliev I, Gerdes A (2022) In-situ LA-ICPMS U–Pb dating of Sulfates: applicability of carbonate reference materials as matrix-matched standards. *Geochronology* 4:601–616. <https://doi.org/10.5194/gchron-4-601-2022>
- Bertrand Ph, Ellis DJ, Green DH (1991) The stability of sapphirine-quartz and hypersthene-sillimanite-quartz assemblages: an experimental investigation in the system FeO–MgO–Al₂O₃–SiO₂ under H₂O and CO₂ conditions. *Contrib Mineral Petrol* 108:55–71
- Brown M, Kothonen FJ (2009) Some remarks on melting and extreme metamorphism of crustal rocks. In: Gupta AK, Dasgupta S (eds) *Phys chem earth*. Springer, New York. https://doi.org/10.1007/978-1-4419-0346-4_4
- Burton KW, Kohn MJ, Cohen AS, O’Nions RK (1995) The relative diffusion of Pb, Nd, Sr and O in garnet. *Earth Planet Sci Lett* 133:199–211
- Carlson RW, Moore RO (2004) Age of the Eastern Kaapvaal mantle: Re–Os isotope data for peridotitic xenoliths from the Monastery kimberlite. *S Afr J Geology* 107:81–90
- Chardon D, Gapais D, Cagnard F (2009) Flow of ultra-hot orogens: a view from the Precambrian, clues for the Phanerozoic. *Tectonophysics* 477(3–4):105–118
- Cherniak DJ, Manchester J, Watson EB (2007) Zr and Hf diffusion in rutile. *Earth Planet Sci Lett* 261(1–2):267–279
- Clark C, Taylor RJM, Kylander-Clark ARC, Hacker BR (2018) Prolonged (>100 Ma) ultrahigh temperature metamorphism in the Napier Complex, East Antarctica: a petrochronological investigation of Earth’s hottest crust. *J Metamorph Geol* 36:1117–1139
- Coward MP, Spencer RM, Spencer CE (1995) Development of the Witwatersrand Basin, South Africa. *Geol Soc, Lond, Spec Publ* 95:243–269. <https://doi.org/10.1144/gsl.sp.1995.095.01.15>
- Dahl PS (1997) A crystal-chemical basis for Pb retention and fission-track annealing systematics in U-bearing minerals, with implications for geochronology. *Earth Planet Sci Lett* 150:277–290
- Dawson JB, Smith JV (1987) Reduced sapphirine granulite xenoliths from the Lace kimberlite, South Africa; implications for the deep structure of the Kaapvaal craton. *Contrib Mineral Petrol* 95:376–383
- Dawson JB, Harley RL, Rudnick RL, Ireland TR (1997) Equilibration and reaction in Archean quartz-sapphirine granulite xenoliths from the Lace kimberlite pipe, South Africa. *J Metamorph Geol* 15:253–266
- Degeling HS (2002) Zircon equilibria in metamorphic rocks. Unpublished PhD thesis, The Australian National University. <https://doi.org/10.25911/5d7784e53bbb6>
- DeWolf CP, Zeissler CJ, Halliday AN, Mezger K, Essene EJ (1996) The role of inclusions in U–Pb and Sm–Nd garnet geochronology: stepwise dissolution experiments and trace uranium mapping by fission track analysis. *Geochim Cosmochim Acta* 60(1):121–134. [https://doi.org/10.1016/0016-7037\(95\)00367-3](https://doi.org/10.1016/0016-7037(95)00367-3)
- Dodson MH (1973) Closure temperature in cooling geochronological and petrological systems. *Contrib Mineral Petrol* 40(3):259–274
- Dohmen R, Marschall HR, Thomas L, Polednia J (2019) Diffusion of Zr, Hf, Nb and Ta in rutile: effects of temperature, oxygen fugacity, and doping level, and relation to rutile point defect chemistry. *Phys Chem Miner* 46:311–332
- Eglinton BM, Armstrong RA (2004) The Kaapvaal Craton and adjacent orogens, southern Africa: a geochronological database and overview of the geological development of the craton. *S Afr J Geol* 107:13–32
- Ellis DJ (1987) Origin and evolution of granulites in normal and thickened crusts. *Geology* 15:167–170
- Ferry JM, Watson EB (2007) New thermodynamic models and revised calibrations for the Ti-in-zircon and Zr-in-rutile thermometers. *Contrib Mineral Petrol* 154:429–437
- Field M, Stiefenhofer J, Robey J, Kurszlauskis S (2008) Kimberlite-hosted diamond deposits of southern Africa: a review. *Ore Geol Rev* 34:33–75
- Firdu FT, Taskinen P (2010) Sulfide mineralogy—literature review. Book chapter, Aalto University Publications in Material Science and Engineering <https://doi.org/10.5382/Mono.04.23>
- Gapais D, Cagnard F, Gueydan F, Barbey P, Ballèvre M (2009) Mountain building and exhumation processes through time: inferences from nature and models. *Terra Nova* 21:188–194
- Gerdes A, Zeh A (2006) Combined U–Pb and Hf Isotope LA-(MC-) ICP-MS analyses of detrital zircons: comparison with SHRIMP and new constraints for the provenance and age of an Armorican Metasediment in Central Germany. *Earth Planet Sci Lett* 249:47–61. <https://doi.org/10.1016/j.epsl.2006.06.039>
- Gerdes A, Zeh A (2009) Zircon formation versus zircon alteration—new insights from combined U–Pb and Lu–Hf in-situ LA-ICP-MS analyses of Archean zircons from the Limpopo Belt. *Chem Geol* 261(3–4):230–243. <https://doi.org/10.1016/j.chemgeo.2008.03.005>
- Hacker BR, Kelemen PB, Behn MD (2011) Differentiation of the continental crust by relamination. *Earth Planet Sci Lett* 307:501–516
- Harley S (2016) A matter of time: the importance of the duration of UHT metamorphism. *J Mineral Petrol Sci* 111:50–72
- Harley S, Kelly NM, Möller A (2007) Zircon behaviour and the thermal histories of mountain chains. *Elements* 3:25–30
- Hart R, Moser D, Andreoli M (1999) Archean age for the granulite facies metamorphism near the center of the Vredefort structure. *S Afr J Geol* 27(12):1091–1094
- Harte B, Jackson PM (1981) Age of mineral equilibria in granulite facies nodules from kimberlites. *Nature* 291:147–148
- Hensen RJ, Green DH (1973) Experimental study of the stability of cordierite and garnet in pelitic compositions at high pressures and temperatures. III synthesis of experimental data and geological applications. *Contrib Mineral Petrol* 38:151–166
- Herzberg C, Condie K, Korenaga J (2010) Thermal history of the Earth and its petrological expression. *Earth Planet Sci Lett* 292(1–2):79–88
- Hodges KV, Crowley PD (1985) Error estimation and empirical geothermobarometry for pelitic systems. *Am Miner* 70:702–709
- Höfer HE, Brey GP (2007) The iron oxidation state of garnet by electron microprobe: its determination with the flank method combined with major-element analysis. *Am Miner* 92(5–6):873–885. <https://doi.org/10.2138/AM.2007.2390>
- Höfer HE, Brey GP, Shu Q, Heckel C, Vasilyev P (2017) Redox state of Archean kyanite/corundum eclogites and garnet pyroxenites from Bellsbank, South Africa. In: *International Kimberlite Conference: Extended Abstracts* <https://doi.org/10.29173/ikc3822>
- Horie K, Hokada T, Hiroi Y, Motoyoshi Y, Shiraishi K (2012) Contrasting Archean crustal records in western part of the Napier complex, East Antarctica: new constraints from SHRIMP geochronology. *Gondwana Res* 21:829–837
- Horstwood MSA, Košler J, Gehrels G, Jackson SE, McLean NM, Paton C, Pearson NJ, Sircombe K, Sylvester P, Vermeesch P, Bowring JF (2016) Community-derived standards for LA-ICP-MS U–(Th–) Pb geochronology-uncertainty propagation, age interpretation and data reporting. *Geostand Geoanal Res* 40:311–332. <https://doi.org/10.1111/j.1751-908X.2016.00379.x>

- Humbert F, Hofmann A, de Kock M, Agangi A, Chou Y-M, Mambane PW (2021) A geochemical study of the Crown Formation and Bird Member lavas of the Mesoarchean Witwatersrand Supergroup South Africa. *S Afr J Geol* 124(3):663–684. <https://doi.org/10.25131/sajg.124.0022>
- Jackson SE, Pearson NJ, Griffin WL, Belousova EA (2004) The application of laser ablation inductively coupled plasma–mass spectrometry to in situ U–Pb zircon geochronology. *Chem Geol* 211:47–69. <https://doi.org/10.1016/j.chemgeo.2004.06.017>
- Jacob DE, Bizimis M, Salters VJM (2005) Lu–Hf and geochemical systematics of recycled ancient oceanic crust: evidence from Roberts Victor eclogites. *Contrib Mineral Petrol* 148:707–720. <https://doi.org/10.1007/s00410-004-0631-x>
- Jochum KP, Weis U, Stoll B, Kuzmin D, Yang Q, Raczek I, Jacob DE, Stracke A, Birbaum K, Frick DA, Günther D, Enzweiler J (2011) Determination of reference values for NIST SRM 610–617 glasses following ISO guidelines. *Geostand Geoanal Res* 35:97–429. <https://doi.org/10.1111/j.1751-908X.2011.00120.x>
- Jochum KP, Weis U, Schwager B, Stoll B, Wilson SA, Haug GH, Andreae MO, Enzweiler J (2016) Reference values following ISO guidelines for frequently requested rock reference materials. *Geostand Geoanal Res* 40:333–350. <https://doi.org/10.1111/j.1751-908X.2015.00392.x>
- Kamo SL, Davis DW (1994) Reassessment of Archean crustal development in the Barberton Mountain Land, South Africa, based on U–Pb dating. *Tectonics* 13:167–192
- Keller DS, Ague LL (2019) Crystallographic and textural evidence for precipitation of rutile, ilmenite, corundum, and apatite lamellae from garnet. *Am Mineral* 104(7):980–995. <https://doi.org/10.2138/am-2019-6849>
- Kelsey D, Hand M (2015) On ultrahigh temperature crustal metamorphism: phase equilibria, trace element thermometry, bulk composition, heat sources, timescales and tectonic settings. *Geosci Front* 6(3):311–356
- Kelsey D, Clark C, Hand M (2008) Thermobarometric modeling of zircon and monazite growth in melt-bearing systems: examples using model metapelitic and metasomatic granulites. *J Metamorph Geol* 26:199–212
- Kitakaze A, Sugaki A, Itoh H, Komatsu R (2011) A revision of phase relations in the system Fe–Ni–S from 650 °C to 450 °C. *Canad Mineral* 49:1687–1710
- Kohn MJ (2016) Metamorphic chronology—a tool for all ages: past achievements and future prospects. *Am Miner* 101:25–42. <https://doi.org/10.2138/am-2016-5146>
- Kohn MJ, Kelly NM (2018) Petrology and geochronology of metamorphic zircon. *Microstructural geochronology*. American Geophysical Union (AGU), pp 35–61. <https://doi.org/10.1002/978119227250.ch2>
- Kohn MJ, Corrie SI, Markley C (2015) The fall and rise of metamorphic zircon. *Am Miner* 100(4):897–908. <https://doi.org/10.2138/am-2015-5064>
- Korhonen FJ, Clark C, Brown M, Bhattacharya S, Taylor R (2013) How long-lived is ultrahigh temperature (UHT) metamorphism? Constraints from zircon and monazite geochronology in the Eastern Ghats orogenic belt, India. *Precamb Res* 234:322–350
- Kozlik M, Raith J, Gerdes A (2016) U–Pb, Lu–Hf and trace element characteristics of zircon from the Felbertal scheelite deposit (Austria): new constraints on timing and source of W mineralization. *Chem Geol* 421:112–126
- Kramers JD, Kreissig K, Jones MQW (2001) Crustal heat production and style of metamorphism: a comparison between two Archean high grade provinces in the Limpopo Belt, southern Africa. *Precamb Res* 112:149–163
- Kullerud G, Yund RA, Moh GH (1969) Phase Relations in the Cu–Fe–S, Cu–Ni–S, and Fe–Ni–S systems. In: Wilson HDB (ed) *Magmatic ore deposits*. Econ Geol Monograph 4: 323–343
- Ludwig KR (2012) *User's Manual for Isoplot Version 3.75-4.15: a Geochronological Toolkit for Microsoft Excel*, Berkeley Geochronological Center Special Publication, 5.
- MacIntyre RM, Dawson JB (1976) Age and significance of some South African kimberlites. Abstract 66 Abstr. 4th Eur. Coll. Geochronol. Isotope Geol., Amsterdam
- Marschall HR, Hawkesworth CJ, Storey CD, Dhuime B, Leat PT, Meyer H-P, Buckle ST (2010) The annandagstoppane granite, East Antarctica: evidence for archaean intracrustal recycling in the Kaapvaal-Grunehogna craton from zircon O and Hf isotopes. *J Petrol* 51(11):2277–2301. <https://doi.org/10.1093/ptrology/egq057>
- McDonough WF, Sun SS (1995) The composition of the earth. *Chem Geol* 120(3–4):223–253
- McLennan SM, Taylor SR, Kröner A (1983) Geochemical evolution of Archean shales from South Africa. I. The Swaziland and Pongola Supergroups. *Precamb Res* 22(1–3):93–124
- Mezger K, Hanson GN, Bohlen SR (1989) U–Pb systematics of garnet: dating the growth of garnet in the Late Archean Pikwitonei granulite domain at Cauchon and Natawahunan Lakes, Manitoba, Canada. *Contrib Mineral Petrol* 101:136–148
- Mezger K, Rawnsley CM, Bohlen SR, Hanson GN (1991) U–Pb garnet, sphene, monazite, and rutile ages: implications for the duration of high-grade metamorphism and cooling histories, Adirondack Mts., New York. *J Geol* 99(3):415–428
- Millonig LJ, Albert R, Gerdes A, Avigad D, Dietsch C (2020) Exploring laser ablation U–Pb dating of regional metamorphic garnet—the Straits Schist, Connecticut, USA. *Earth Planet Sci Lett* 552:116589. <https://doi.org/10.1016/j.epsl.2020.116589>
- Moser DE, Flowers RM, Hart RJ (2001) Birth of the Kaapvaal tectosphere 3.08 billion years ago. *Science* 291:465–468
- Norris A, Danyushevsky L (2018) Towards estimating the complete uncertainty budget of quantified results measured by LAICP-MS. Goldschmidt, Boston
- Pape J, Mezger K, Robyr M (2016) A systematic evaluation of the Zr-in-rutile thermometer in ultra-high temperature (UHT) rocks. *Contrib Mineral Petrol* 171:44–62. <https://doi.org/10.1007/s00410-016-1254-8>
- Paprika D, Hofmann A, Agangi A, Elburg M, Xie H (2021) Age of the Dominion-Nsuze Igneous Province, the first intracratonic Igneous Province of the Kaapvaal Craton. *Precamb Res* 363(3–4):106335. <https://doi.org/10.1016/j.precamres.2021.106335>
- Pauly J, Marschall HR, Meyer H-P, Chatterjee N, Monteleone B (2016) Prolonged Ediacaran–Cambrian metamorphic history and short-lived high-pressure granulite-facies metamorphism in the HU Sverdrupfjella, Dronning Maud Land (East Antarctica): evidence for continental collision during Gondwana Assembly. *J Petrol* 57(1):185–228. <https://doi.org/10.1093/ptrology/egw005>
- Pearson DG, Wittig N (2008) Formation of Archean continental lithosphere and its diamonds: the root of the problem. *J Geol Soc Lond* 165:895–914
- Pearson NJ, O'Reilly SY, Griffin WL (1995) The crust-mantle boundary beneath cratons and craton margins: a transect across the south-west margin of the Kaapvaal craton. *Lithos* 36:257–287
- Pollington A, Baxter E (2010) High resolution Sm–Nd garnet geochronology reveals the uneven pace of tectonometamorphic processes. *Earth Planet Sci Lett* 293:63–71. <https://doi.org/10.1016/J.EPSL.2010.02.019>
- Poujol M, Robb LJ, Anhaeusser CR, Gericke B (2003) A review of the geochronological constraints on the evolution of the Kaapvaal Craton, South Africa. *Precamb Res* 127:181–213

- Richardson S, Gurney J, Erlank A, Harris J (1984) Origin of diamonds in old enriched mantle. *Nature* 310:198–202
- Rubatto D (2002) Zircon trace element geochemistry: partitioning with garnet and the link between U–Pb ages and metamorphism. *Chem Geol* 184:123–138
- Rubatto D, Hermann J (2007) Experimental zircon/melt and zircon/garnet trace element partitioning and implications for the geochronology of crustal rocks. *Chem Geol* 241:38–61
- Rybach L (1988) Determination of heat production rate. In: Hänel R, Rybach L, Stegena L (eds) *Handbook of terrestrial heat flow density determination*. Kluwer, Dordrecht, pp 125–142
- Santos MM, Lana C, Scholz R, Buick I, Schmitz MD, Kamo SL, Gerdes A, Corfu F, Tapster S, Lancaster P, Storey CD, Basei MA, Tohver E, Alkmim A, Nalini H, Krambrock K, Fantini C, Wiedenbeck M (2017) A new appraisal of Sri Lankan BB Zircon as a reference material for LA-ICP-MS U–Pb geochronology and Lu–Hf isotope tracing. *Geost and Geoanal Res* 41(3):335–358. <https://doi.org/10.1111/ggr.12167>
- Schannon M, Lana C, Nicoli G, Cutts K, Buick I, Gerdes A, Hecht L (2021) Reconstructing the metamorphic evolution of the Araçuaí orogen (SE Brazil) using in situ U–Pb garnet dating and P–T modelling. *J Metamorph Geol* 39(9):1145–1171
- Schmitz MD, Bowring SA (2003a) Ultrahigh-temperature metamorphism in the lower crust during Neoproterozoic Ventersdorp rifting and magmatism, Kaapvaal Craton, southern Africa. *GSA Bull* 115(5):533–548
- Schmitz MD, Bowring SA (2003b) Constraints on the thermal evolution of continental lithosphere from U–Pb accessory mineral thermochronometry of lower crustal xenoliths, southern Africa. *Contrib Mineral Petrol* 144:592–618
- Schmitz MD, Bowring SA (2004) Lower crustal granulite formation during Mesoproterozoic Namaqua–Natal collisional orogenesis, southern Africa. *S Afr J Geol* 107:261–284
- Schoene B, de Wit M, Bowring SA (2008) Mesoarchean assembly and stabilization of the eastern Kaapvaal craton: a structural-thermochronological perspective. *Tectonics* 27:1–27
- Seman S, Stockli DF, McLean NM (2017) U–Pb geochronology of grossular-andradite garnet. *Chem Geol* 460:106–116. <https://doi.org/10.1016/j.chemgeo.2017.04.020>
- Slama J, Kosler J, Condon DJ, Crowley JL, Gerdes A, Hanchar JM, Horstwood MSA, Morris GA, Nasdala L, Norberg N, Schaltegger U, Schoene B, Tubrett MN, Whitehouse MJ (2008) Plesovice zircon—a new natural reference material for U–Pb and Hf isotopic microanalysis. *Chem Geol* 249:1–35. <https://doi.org/10.1016/j.chemgeo.2007.11.005>
- Sommer H, Wan Y, Kröner A, Xie H, Jacob DE (2013) SHRIMP zircon ages and petrology of lower crustal granulite xenoliths from the Letseng-La-Terae kimberlite, Lesotho. Further evidence for a Namaqua Natal connection. *S Afr J Geol* 116(2):183–198. <https://doi.org/10.2113/gssajg.116.2.183>
- Spear FS, Peacock SM, Kohn MJ, Florence FP, Menard T (1991) Computer programs for petrologic P–T–t path calculations. *Am Miner* 76:2009–2012
- Stevens G, Gibson RL, Droop GTR (1997) Mid-crustal granulite facies metamorphism in the Central Kaapvaal craton: the Bushveld Complex connection. *Precamb Res* 82:113–132
- Suhr N, Hoffmann JE, Kröner A (2015) Archaean granulite-facies paragneisses from central Swaziland: Inferences on Palaeoarchaean crustal reworking and a complex metamorphic history. *J Geol Soc, Lond* 172:139–152
- Suzuki S, Arima M, Williams IS, Shiraishi K, Kagami H (2006) Thermal history of UHT metamorphism in the Napier Complex, East Antarctica: insights from zircon, monazite and garnet ages. *J Geol* 114:65–84
- Taylor-Jones K, Powell R (2015) Interpreting zirconium-in-rutile thermometric results. *J Metamorph Geol* 33(2):115–122. <https://doi.org/10.1111/jmg.12109>
- Taylor RJM, Harley SL, Hinton RW, Elphick S, Clark C, Kelley NM (2015) Experimental determination of REE partition coefficients between zircon, garnet and melt: a key to understanding high-T crustal processes. *J Metamorph Geol* 33:231–248
- Tera F, Wasserburg GJ (1972) U–Th–Pb systematics in three Apollo 14 basalts and the problem of initial Pb in lunar rocks. *Earth Planet Sci Lett* 14:281–304. [https://doi.org/10.1016/0012-821X\(72\)90128-8](https://doi.org/10.1016/0012-821X(72)90128-8)
- Thomas RJ, von Weh MW, McCourt S (1993) The tectonic evolution of southern Africa: an overview. *J Afr Earth Sci* 16(1–2):5–24
- Toulkeridis T, Clauer N, Kröner A, Todt W (2015) Mineralogy, geochemistry and isotope dating of shales from the Barberton Greenstone belt, South Africa: provenance and tectonic implications. *S Afr J Geol* 118(4):389–410
- Tual L, Matthijs AS, Kooijman E, Kielman-Schmitt L, Ratschbacher L (2022) Garnet, zircon, and monazite age and REE signatures in (ultra)high-temperature and high-pressure rocks: examples from the Caledonides and the Pamir. *J Metamorph Geol* 40:1321–1346. <https://doi.org/10.1111/jmg.12667>
- Van der Westhuizen WA, de Bruijn H, Meintjes PG (1991) The Ventersdorp Supergroup: an overview. *J Afr Earth Sci* 13:83–105
- Vermeesch P (2012) On the visualisation of detrital age distributions. *Chem Geol* 312–313:190–194. <https://doi.org/10.1016/j.chemgeo.2012.04.0210>
- Wafform S, Seman S, Kyle JR, Stockli D, Leys C, Sonbait D, Cloos M (2018) Andradite garnet U–Pb geochronology of the Big Gossan skarn, Ertsberg-Grasberg Mining district, Indonesia. *Econ Geol* 113:769–778
- Watson EB, Wark DA, Thomas JB (2006) Crystallization thermometers for zircon and rutile. *Contrib Mineral Petrol* 151:413–433
- Yakymchuk C (2023) Prograde zircon growth in migmatites. *J Metamorph Geol* 41:719–743
- Yang Y-H, Wu F-Y, Yang J-H, Mitchell RH, Zhao Z-F, Xie L-W, Huang C, Yang M, Zhao H (2018) U–Pb age determination of schorlomite garnet by laser ablation inductively coupled plasma mass spectrometry. *J Anal at Spectrom* 33:231–239
- Yund RA, Kullerud G (1966) Thermal stability of assemblages in the Cu–Fe–S system. *J Petrol* 7(3):454–488. <https://doi.org/10.1093/petrology/7.3.454>
- Zack T, Moraes R, Kronz A (2004) Temperature dependence of Zr in rutile: empirical calibration of a rutile thermometer. *Contrib Mineral Petrol* 148:471–488